Supplementary Materials for "Risk of Upgrading Based Personalized Biopsy Schedules for Prostate Cancer Active Surveillance Patients"

Anirudh Tomer, MSc[a,*], Daan Nieboer, MSc[b], Monique J. Roobol, PhD[c], Anders Bjartell, MD, PhD[d], Ewout W. Steyerberg, PhD[b,e], Dimitris Rizopoulos, PhD[a], Movember Foundation's Global Action Plan Prostate Cancer Active Surveillance (GAP3) consortium[f]

[a]*Department of Biostatistics, Erasmus University Medical Center, Rotterdam, the Netherlands*
[b]*Department of Public Health, Erasmus University Medical Center, Rotterdam, the Netherlands*
[c]*Department of Urology, Erasmus University Medical Center, Rotterdam, the Netherlands*
[d]*Department of Urology, Skåne University Hospital, Malmö, Sweden*
[e]*Department of Biomedical Data Sciences, Leiden University Medical Center, Leiden, the Netherlands*
[f]*The Movember Foundation's Global Action Plan Prostate Cancer Active Surveillance (GAP3) consortium members presented in Appendix F*

Appendix A. A Joint Model for the Longitudinal PSA, and Time to Gleason Upgrading

Let T_i^* denote the true time of upgrading (increase in biopsy Gleason grade group from 1 to 2 or higher) for the i-th patient included in PRIAS. Since biopsies are conducted periodically, T_i^* is observed with interval censoring $l_i < T_i^* \leq r_i$. When upgrading is observed for the patient at his latest

*Corresponding author (Anirudh Tomer): Erasmus MC, kamer flex Na-2823, PO Box 2040, 3000 CA Rotterdam, the Netherlands. Tel: +31 10 70 43393

Email addresses: a.tomer@erasmusmc.nl (Anirudh Tomer, MSc), d.nieboer@erasmusmc.nl (Daan Nieboer, MSc), m.roobol@erasmusmc.nl (Monique J. Roobol, PhD), anders.bjartell@med.lu.se (Anders Bjartell, MD, PhD), e.w.steyerberg@lumc.nl (Ewout W. Steyerberg, PhD), d.rizopoulos@erasmusmc.nl (Dimitris Rizopoulos, PhD)

biopsy time r_i, then l_i denotes the time of the second latest biopsy. Otherwise, l_i denotes the time of the latest biopsy and $r_i = \infty$. Let $\boldsymbol{y}_i$ denote his observed PSA longitudinal measurements. The observed data of all n patients is denoted by $\mathcal{A}_n = \{l_i, r_i, \boldsymbol{y}_i; i = 1, \ldots, n\}$.

In our joint model, the patient-specific PSA measurements over time are modeled using a linear mixed effects sub-model. It is given by (see Panel A, Figure 1):

$$\begin{aligned} \log_2\big\{y_i(t)+1\big\} &= m_i(t) + \varepsilon_i(t), \\ m_i(t) &= \beta_0 + b_{0i} + \sum_{k=1}^{4}(\beta_k + b_{ki})B_k\Big(\frac{t-2}{2}, \frac{\mathcal{K}-2}{2}\Big) + \beta_5 \text{age}_i, \end{aligned} \tag{1}$$

where, $m_i(t)$ denotes the measurement error free value of $\log_2(\text{PSA}+1)$ transformed [2, 3] measurements at time t. We model it non-linearly over time using B-splines [4]. To this end, our B-spline basis function $B_k\{(t-2)/2, (\mathcal{K}-2)/2\}$ has three internal knots at $\mathcal{K} = \{0.5, 1.3, 3\}$ years, which are the three quartiles of the observed follow-up times. The boundary knots of the spline are at 0 and 6.3 years (95-th percentile of the observed follow-up times). We mean centered (mean 2 years) and standardized (standard deviation 2 years) the follow-up time t and the knots of the B-spline $\mathcal{K}$ during parameter estimation for better convergence. The fixed effect parameters are denoted by $\{\beta_0, \ldots, \beta_5\}$, and $\{b_{0i}, \ldots, b_{4i}\}$ are the patient specific random effects. The random effects follow a multivariate normal distribution with mean zero and variance-covariance matrix $\boldsymbol{W}$. The error $\varepsilon_i(t)$ is assumed to be t-distributed with three degrees of freedom (see Appendix B.1) and scale σ, and is independent of the random effects.

To model the impact of PSA measurements on the risk of upgrading, our joint model uses a relative risk sub-model. More specifically, the hazard of upgrading denoted as $h_i(t)$, and the cumulative-risk of upgrading denoted as $R_i(t)$, at a time t are (see Panel C, Figure 1):

$$\begin{aligned} h_i(t) &= h_0(t)\exp\Big(\gamma \text{age}_i + \alpha_1 m_i(t) + \alpha_2 \frac{\mathrm{d}m_i(t)}{\mathrm{d}t}\Big), \\ R_i(t) &= \exp\Big\{-\int_0^t h_i(s)\mathrm{d}s\Big\}, \end{aligned} \tag{2}$$

where, γ is the parameter for the effect of age. The impact of PSA on the hazard of upgrading is modeled in two ways, namely the impact of the error

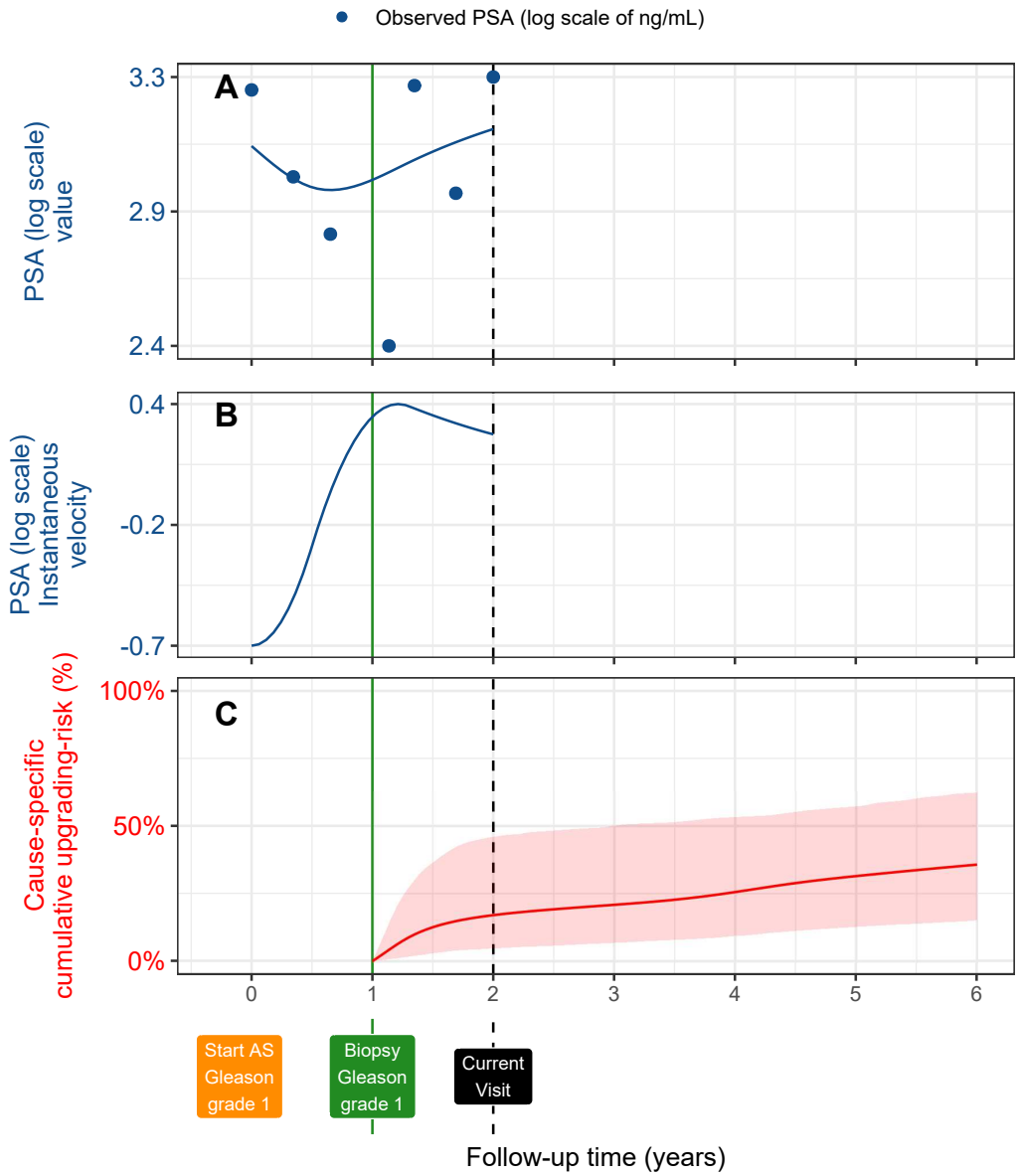

Figure 1: **Illustration of the joint model on a real PRIAS dataset patient**. **Panel A:** Observed (blue dots) and fitted PSA (solid blue line) measurements, log-transformed. **Panel B:** Estimated instantaneous velocity of PSA (log-transformed). **Panel C**: Predicted cumulative-risk of upgrading (95% credible interval shaded). Upgrading is defined as an increase in Gleason grade group [1] from grade group 1 to 2 or higher. This risk of upgrading is available starting from the time of the latest negative biopsy (vertical green line at year 1 of follow-up). The joint model estimated it by combining the fitted PSA value and velocity (both on the log scale of PSA) and time of the latest negative biopsy. Black dashed line at year 4 denotes the time of current visit.

free underlying PSA value $m_i(t)$ (see Panel A, Figure 1), and the impact of the underlying PSA velocity $\mathrm{d}m_i(t)/\mathrm{d}t$ (see Panel B, Figure 1). The corresponding parameters are α_1 and α_2, respectively. Lastly, $h_0(t)$ is the baseline hazard at time t, and is modeled flexibly using P-splines [5]. More specifically:

$$\log h_0(t) = \gamma_{h_0,0} + \sum_{q=1}^{Q} \gamma_{h_0,q} B_q(t, \boldsymbol{v}),$$

where $B_q(t, \boldsymbol{v})$ denotes the q-th basis function of a B-spline with knots $\boldsymbol{v} = v_1, \ldots, v_Q$ and vector of spline coefficients γ_{h_0}. To avoid choosing the number and position of knots in the spline, a relatively high number of knots (e.g., 15 to 20) are chosen and the corresponding B-spline regression coefficients γ_{h_0} are penalized using a differences penalty [5].

We estimate the parameters of the joint model using Markov chain Monte Carlo (MCMC) methods under the Bayesian framework. Let $\boldsymbol{\theta}$ denote the vector of all of the parameters of the joint model. The joint model postulates that given the random effects, the time of upgrading, and the PSA measurements taken over time are all mutually independent. Under this assumption the posterior distribution of the parameters is given by:

$$\begin{aligned} p(\boldsymbol{\theta}, \boldsymbol{b} \mid \mathcal{A}_n) &\propto \prod_{i=1}^{n} p(l_i, r_i, \boldsymbol{y}_i, \mid \boldsymbol{b}_i, \boldsymbol{\theta}) p(\boldsymbol{b}_i \mid \boldsymbol{\theta}) p(\boldsymbol{\theta}) \\ &\propto \prod_{i=1}^{n} p(l_i, r_i \mid \boldsymbol{b}_i, \boldsymbol{\theta}) p(\boldsymbol{y}_i \mid \boldsymbol{b}_i, \boldsymbol{\theta}) p(\boldsymbol{b}_i \mid \boldsymbol{\theta}) p(\boldsymbol{\theta}), \\ p(\boldsymbol{b}_i \mid \boldsymbol{\theta}) &= \frac{1}{\sqrt{(2\pi)^q \det(\boldsymbol{W})}} \exp\Big\{ -\frac{1}{2} (\boldsymbol{b}_i^T \boldsymbol{W}^{-1} \boldsymbol{b}_i) \Big\}, \end{aligned}$$

where, the likelihood contribution of the PSA outcome, conditional on the random effects is:

$$p(\boldsymbol{y}_i \mid \boldsymbol{b}_i, \boldsymbol{\theta}) = \frac{1}{\left(\sqrt{2\pi\sigma^2}\right)^{n_i}} \exp\Big\{ -\frac{\sum_{j=1}^{n_i} (y_{ij} - m_{ij})^2}{2\sigma^2} \Big\},$$

where n_i is the number of PSA measurements of the i-th patient. The likelihood contribution of the time of upgrading outcome is given by:

$$p(l_i, r_i \mid \boldsymbol{b}_i, \boldsymbol{\theta}) = \exp\Big\{ -\int_0^{l_i} h_i(s) \mathrm{d}s \Big\} - \exp\Big\{ -\int_0^{r_i} h_i(s) \mathrm{d}s \Big\}. \qquad (3)$$

The integrals in (3) do not have a closed-form solution, and therefore we use a 15-point Gauss-Kronrod quadrature rule to approximate them.

We use independent normal priors with zero mean and variance 100 for the fixed effects $\{\beta_0, \ldots, \beta_5\}$, and inverse Gamma prior with shape and rate both equal to 0.01 for the parameter σ^2. For the variance-covariance matrix $\boldsymbol{W}$ of the random effects, we take inverse Wishart prior with an identity scale matrix and degrees of freedom equal to 5 (number of random effects). For the relative risk model's parameter γ and the association parameters α_1, α_2, we use independent normal priors with zero mean and variance 100.

Appendix A.1. Assumption of t-distributed (df=3) Error Terms

With regards to the choice of the distribution for the error term ε for the PSA measurements (see Equation 1), we attempted fitting multiple joint models differing in error distribution, namely t-distribution with three, and four degrees of freedom, and a normal distribution for the error term. However, the model assumption for the error term was best met by the model with t-distribution having three degrees of freedom. The quantile-quantile plot of subject-specific residuals for the corresponding model in Panel A of Figure 2, shows that the assumption of t-distributed (df=3) errors is reasonably met by the fitted model.

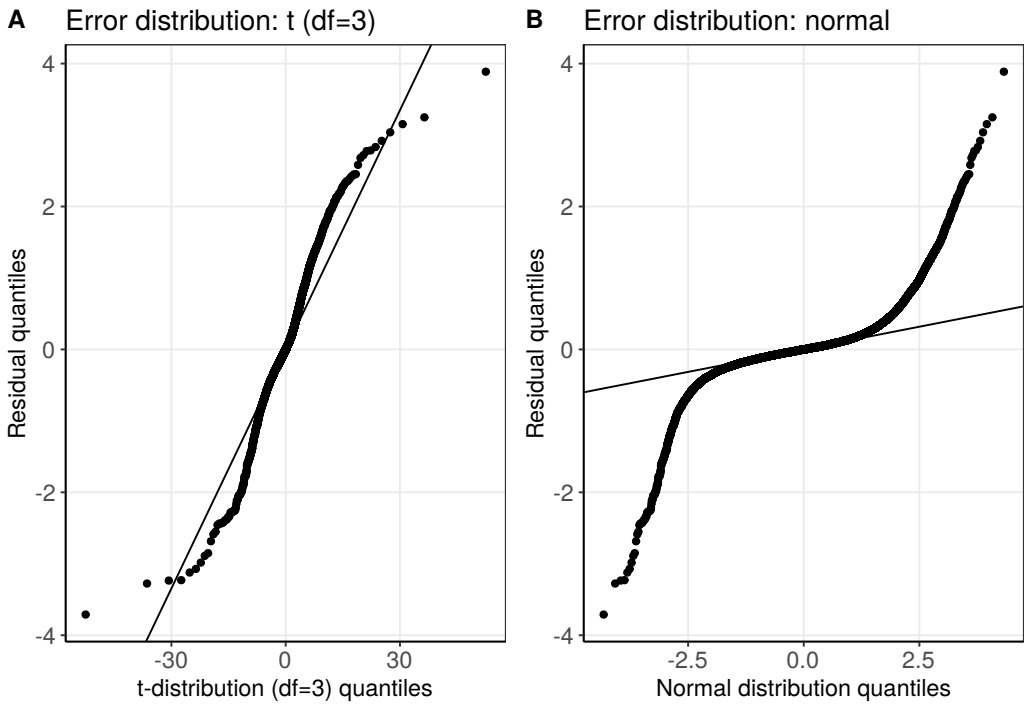

Figure 2: **Quantile-quantile plot** of subject-specific PSA residuals from two different joint models fitted to the PRIAS dataset. **Panel A**: model assuming a t-distribution (df=3) for the error term ε (see Equation 1). **Panel B**: model assuming a normal distribution for the error term ε. We selected the model with t-distributed error terms.

Appendix A.2. PSA Dependent Biopsy Schedule of PRIAS, and Competing Risks

PSA dependent interval censored time of upgrading: The true time of upgrading T_i^* is not known for any of the patients in PRIAS. In order to detect upgrading, PRIAS uses a fixed schedule of biopsies wherein biopsies are conducted at year one, year four, year seven and year ten of follow-up, and every five years thereafter. However, PRIAS switches to a more frequent annual biopsy schedule for faster-progressing patients. These are patients with PSA doubling time (PSA-DT) between 0 and 10 years, which is measured as the inverse of the slope of the regression line through the base two logarithm of PSA values. Thus, the interval $l_i < T_i^* \leq r_i$ in which upgrading is detected depends on the observed PSA values.

Competing events: The primary event of interest in this paper is upgrading observed via a positive biopsy. There are three types of competing events, namely death, removal of patients from AS on the basis of their observed DRE and PSA measurements, watchful-waiting, and loss to follow-up of patients because of patient anxiety or unknown reasons.

The number of patients obtaining the event death is small compared to the number of patients who obtain the primary event upgrading. Hence in this paper considering death as non-informative censoring may be viable. We also consider loss to follow-up as non-informative censoring, which may not always be true. This is especially the case when the reason of loss to follow-up is unknown. However, when the reason of loss to follow-up is patient anxiety, it is often on the basis of their observed results. Given the large number of loss to follow-up patients, considering these patients as censored is a limitation of our work. However, the problem of unknown reason of dropout is not specific to only our model. For the remaining patients who are removed from AS on the basis their observed longitudinal data (e.g, treatment, watchful-waiting), in the next paragraph we show that the removal of these patients is non-informative about the parameters of the model for the true time of upgrading.

Given the aforementioned issues of PSA dependent interval censoring and removal of patients on the basis of their observed longitudinal data is natural to question in this scenario if the parameters of the joint model are affected by these two. However, because the parameters of the joint model are estimated using a full likelihood approach [6], the joint model allows the schedule of biopsies, as well as censoring to depend upon the observed PSA measurements (e.g., via PSA-DT), under the condition that the model is correctly

specified. To show this, consider the following full general specification of the joint model that we use. Let $\boldsymbol{y}_i$ denote the observed PSA measurements for the i-th patient, and l_i, r_i denote the two time points of the interval in which upgrading occurs for the i-th patient. In addition let T_i^S and $\mathcal{V}_i$ denote the schedule of biopsies, and the schedule PSA measurements, respectively. Let G_i^* denote the time of removal from AS without observing upgrading. Under the assumption that $T_i^S, G_i^*, \mathcal{V}_i$ may depend upon only the observed data $\boldsymbol{y}_i$, the joint likelihood of the various processes is given by:

$$p(\boldsymbol{y}_i, l_i, r_i, T_i^S, G_i^*, \mathcal{V}_i \mid \boldsymbol{\theta}, \boldsymbol{\psi}) = p(\boldsymbol{y}_i, l_i, r_i \mid \boldsymbol{\theta}) \times p(T_i^S, G_i^*, \mathcal{V}_i \mid \boldsymbol{y}_i, \boldsymbol{\psi}).$$

where, $\boldsymbol{\psi}$ is the vector of parameters for the processes $T_i^S, G_i^*, \mathcal{V}_i$. From this decomposition we can see that even if the processes $T_i^S, G_i^*, \mathcal{V}_i$ may be determined from $\boldsymbol{y}_i$, if we are interested in the parameters $\boldsymbol{\theta}$ of the joint distribution of longitudinal and event outcomes, we can maximize the likelihood based on the first term and ignore the second term. In other words, the second term will not carry information for $\boldsymbol{\theta}$. Lastly, since we use a full likelihood approach with an interval censoring specification, the estimates that we obtain are consistent and asymptotically unbiased [7], despite the interval censoring observed.

Appendix A.3. Results

Characteristics of the six validation cohorts from the GAP3 database [8] are shown in Table 1, Table 2, and Table 3. The cause-specific cumulative upgrading-risk in these cohorts is shown in Figure 3.

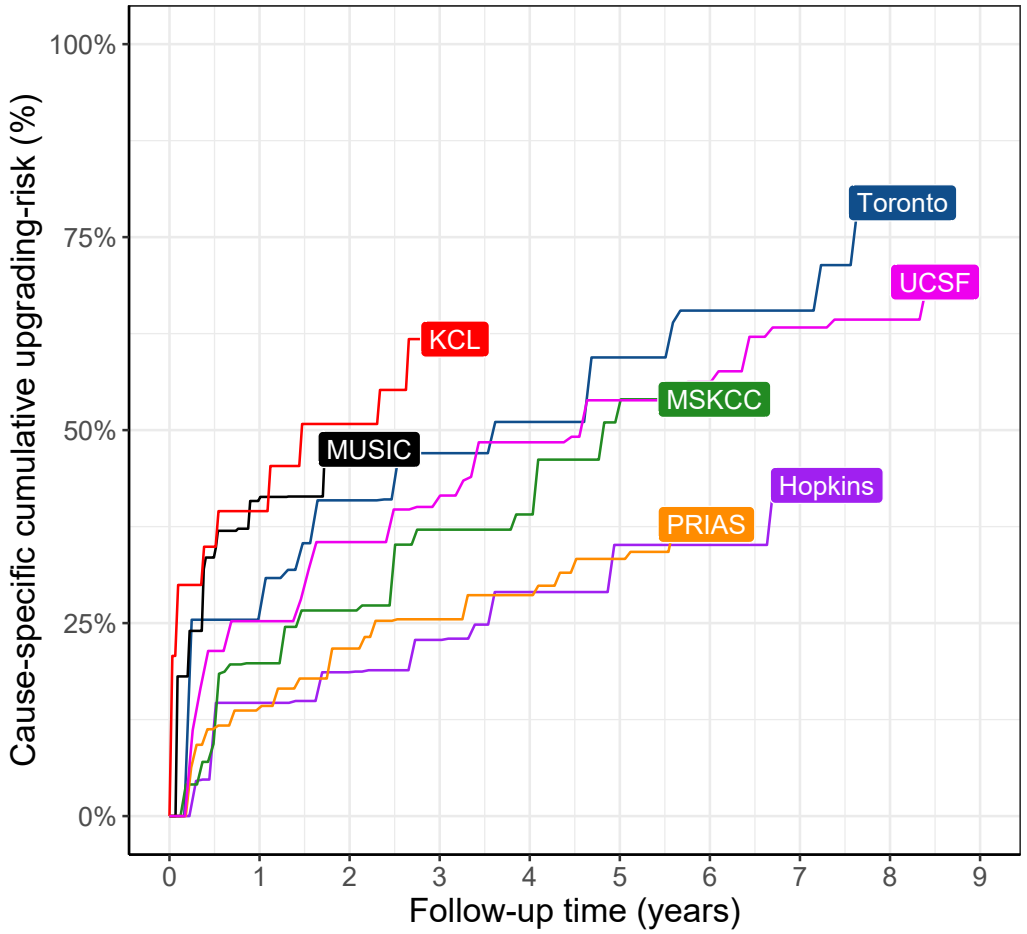

Figure 3: **Nonparametric estimate [9] of the cause-specific cumulative upgrading-risk** in the world's largest AS cohort PRIAS, and largest six AS cohorts from the GAP3 database [8]. Abbreviations are *Hopkins*: Johns Hopkins Active Surveillance, *PRIAS*: Prostate Cancer International Active Surveillance, *Toronto*: University of Toronto Active Surveillance, *MSKCC*: Memorial Sloan Kettering Cancer Center Active Surveillance, *KCL*: King's College London Active Surveillance, *MUSIC*: Michigan Urological Surgery Improvement Collaborative AS, *UCSF*: University of California San Francisco Active Surveillance.

Table 1: **Summary of the Hopkins and Toronto validation cohorts from the GAP3 database [8]**. The primary event of interest is upgrading, that is, increase in Gleason grade group from group 1 to 2 or higher. #PSA: number of PSA, #biopsies: number of biopsies, IQR: interquartile range, PSA: prostate-specific antigen. Full names of cohorts are *Hopkins*: Johns Hopkins Active Surveillance, *Toronto*: University of Toronto Active Surveillance

Characteristic	**Hopkins**	**Toronto**
Total patients	1392	1046
Upgrading (primary event)	260	359
Median age (years)	62 (IQR: 66–69)	67 (IQR: 60–72)
Median maximum follow-up per patient (years)	3 (IQR: 1.3–5.8)	4.5 (IQR: 1.9–8.4)
Total PSA measurements	11126	13984
Median #PSA per patient	6 (IQR: 4–11)	12 (IQR: 7–19)
Median PSA (ng/mL)	4.7 (IQR: 2.9–6.7)	6 (IQR: 3.7–9.0)
Total biopsies	1926	909
Median #biopsies per patient	1 (IQR: 1–2)	1 (IQR: 1–2)

Table 2: **Summary of the MSKCC and UCSF validation cohorts from the GAP3 database [8]**. The primary event of interest is upgrading, that is, increase in Gleason grade group from group 1 to 2 or higher. #PSA: number of PSA, #biopsies: number of biopsies, IQR: interquartile range, PSA: prostate-specific antigen. Full names of cohorts are *MSKCC*: Memorial Sloan Kettering Cancer Center Active Surveillance, *UCSF*: University of California San Francisco Active Surveillance.

Characteristic	**MSKCC**	**UCSF**
Total patients	894	1397
Upgrading (primary event)	242	547
Median age (years)	63 (IQR: 57–68)	63 (IQR: 57–68)
Median maximum follow-up per patient (years)	5.3 (IQR: 1.8–8.3)	3.6 (IQR: 1.5–7.2)
Total PSA measurements	10704	16093
Median #PSA per patient	11 (IQR: 5–17)	8 (IQR: 4–16)
Median PSA (ng/mL)	4.7 (IQR: 2.8–7.1)	5.0 (IQR: 3.4–7.2)
Total biopsies	1102	3512
Median #biopsies per patient	1 (IQR: 1–2)	2 (IQR: 2–3)

Table 3: **Summary of the MUSIC and KCL validation cohorts from the GAP3 database [8]**. The primary event of interest is upgrading, that is, increase in Gleason grade group from group 1 to 2 or higher. #PSA: number of PSA, #biopsies: number of biopsies, IQR: interquartile range, PSA: prostate-specific antigen. Full names of cohorts are *KCL*: King's College London Active Surveillance, *MUSIC*: Michigan Urological Surgery Improvement Collaborative AS.

Characteristic	**MUSIC**	**KCL**
Total patients	2743	616
Upgrading (primary event)	385	198
Median age (years)	65 (IQR: 60–71)	63 (IQR: 58–68)
Median maximum follow-up per patient (years)	1.2 (IQR: 0.6–2.2)	2.4 (IQR: 1.3–3.8)
Total PSA measurements	12087	2987
Median #PSA per patient	4 (IQR: 2–6)	4 (IQR: 2–6)
Median PSA (ng/mL)	5.1 (IQR: 3.4–7.1)	6 (IQR: 4–9)
Total biopsies	1032	484
Median #biopsies per patient	1 (IQR: 1–1)	1 (IQR: 1–1)

Table 4: **Estimated variance-covariance matrix $\boldsymbol{W}$** of the random effects $\boldsymbol{b} = (b_0, b_1, b_2, b_3, b_4)$ from the joint model fitted to the PRIAS dataset. The variances of the random effects are highlighted along the diagonal of the variance-covariance matrix.

Random Effects	b_0	b_1	b_2	b_3	b_4
b_0	**0.229**	0.030	0.023	0.073	0.007
b_1	0.030	**0.149**	0.098	0.171	0.085
b_2	0.023	0.098	**0.276**	0.335	0.236
b_3	0.073	0.171	0.335	**0.560**	0.359
b_4	0.007	0.085	0.236	0.359	**0.351**

The joint model was fitted using the R package **JMbayes** [10]. This package utilizes the Bayesian methodology to estimate model parameters. The corresponding posterior parameter estimates are shown in Table 5 (longitudinal sub-model for PSA outcome) and Table 6 (relative risk sub-model). The parameter estimates for the variance-covariance matrix $\boldsymbol{W}$ from the longitudinal sub-model for PSA are shown in the following Table 4:

For the PSA mixed effects sub-model parameter estimates (see Equation 1), in Table 5 we can see that the age of the patient trivially affects the baseline $\log_2(\text{PSA} + 1)$ measurement. Since the longitudinal evolution of $\log_2(\text{PSA} + 1)$ measurements is modeled with non-linear terms, the interpretation of the coefficients corresponding to time is not straightforward. In lieu of the interpretation, in Figure 4 we present plots of observed versus fitted

Table 5: **Parameters of the longitudinal sub-model**: Estimated mean and 95% credible interval for parameters in Equation (1).

Variable	Mean	Std. Dev	2.5%	97.5%	P
Intercept	2.129	0.060	2.009	2.244	<0.001
Age	0.008	0.001	0.007	0.010	<0.001
Spline: [0.0, 0.5] years	0.063	0.007	0.051	0.075	<0.001
Spline: [0.5, 1.3] years	0.196	0.010	0.177	0.217	<0.001
Spline: [1.3, 3.0] years	0.244	0.014	0.217	0.272	<0.001
Spline: [3.0, 6.3] years	0.382	0.014	0.356	0.410	<0.001
σ	0.139	0.001	0.138	0.140	

Table 6: **Parameters of the relative risk sub-model**: Estimated mean and 95% credible interval for the parameters in Equation (2).

Variable	Mean	Std. Dev	2.5%	97.5%	P
Age	0.037	0.006	0.025	0.049	<0.001
Fitted $\log_2(\text{PSA}+1)$ value	-0.012	0.076	-0.164	0.135	0.856
Fitted $\log_2(\text{PSA}+1)$ velocity	2.266	0.299	1.613	2.767	<0.001

PSA profiles for nine randomly selected patients.

For the relative risk sub-model (see Equation 2), the parameter estimates in Table 6 show that $\log_2(\text{PSA}+1)$ velocity and age of the patient were significantly associated with the hazard of upgrading.

It is important to note that since age, and $\log_2(\text{PSA}+1)$ value and velocity are all measured on different scales, a comparison between the corresponding parameter estimates is not easy. To this end, in Table 7, we present the hazard ratio of upgrading, for an increase in the aforementioned variables from their 25-th to the 75-th percentile. For example, an increase in fitted $\log_2(\text{PSA}+1)$ velocity from -0.085 to 0.308 (fitted 25-th and 75-th percentiles) corresponds to a hazard ratio of 2.433. The interpretation of the rest is similar.

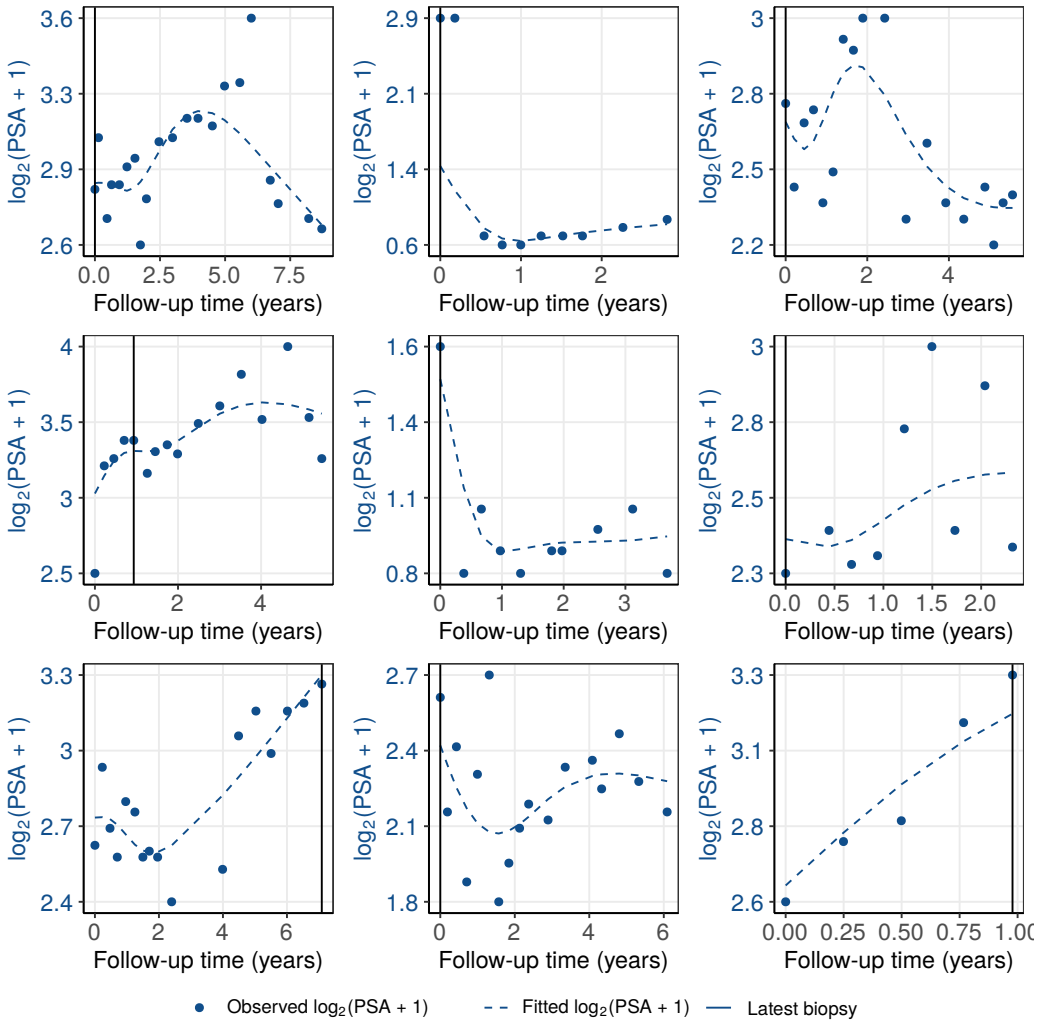

Figure 4: **Fitted versus observed** $\log_2(\mathbf{PSA}+1)$ **profiles** for nine randomly selected PRIAS patients. The fitted profiles utilize information from the observed PSA measurements, and time of the latest biopsy.

Table 7: **Hazard ratio and 95% credible interval (CI) for upgrading**: Variables are on different scale and hence we compare an increase in the variables of relative risk sub-model from their 25-th percentile (P_{25}) to their 75-th percentile (P_{75}). Except for age, quartiles for all other variables are based on their fitted values obtained from the joint model fitted to the PRIAS dataset.

Variable	P_{25}	P_{75}	Hazard ratio [95% CI]
Age	61	71	1.455 [1.285, 1.631]
Fitted $\log_2(\text{PSA}+1)$ value	2.360	3.078	0.991 [0.889, 1.102]
Fitted $\log_2(\text{PSA}+1)$ velocity	-0.085	0.308	2.433 [1.883, 2.962]

Table 8: **Parameters of the relative risk sub-model in validation cohorts**. We fitted separate joint models for each of the six GAP3 validation cohorts as well. The specification of these joint models was same as that of the model for PRIAS. Two important predictors in the relative-risk sub-model, namely, the $\log_2(\text{PSA}+1)$ value and velocity have different impact on upgrading-risk across the cohorts. Table shows the mean estimate of these parameters with 95% credible interval in brackets. Strongest average effect of $\log_2(\text{PSA}+1)$ velocity is in PRIAS cohort, whereas the weakest is in MUSIC cohort. The strongest average effect of $\log_2(\text{PSA}+1)$ value is in the Toronto cohort whereas the weakest is in PRIAS cohort. Full names of cohorts are *Hopkins*: Johns Hopkins Active Surveillance, *PRIAS*: Prostate Cancer International Active Surveillance, *Toronto*: University of Toronto Active Surveillance, *MSKCC*: Memorial Sloan Kettering Cancer Center Active Surveillance, *KCL*: King's College London Active Surveillance, *MUSIC*: Michigan Urological Surgery Improvement Collaborative AS, *UCSF*: University of California San Francisco Active Surveillance.

Cohort	Fitted $\log_2(\text{PSA}+1)$ value	Fitted $\log_2(\text{PSA}+1)$ velocity
PRIAS	-0.012 [-0.164, 0.135]	2.266 [1.613, 2.767]
Hopkins	0.061 [-0.323, 0.329]	1.839 [0.761, 4.378]
MSKCC	0.336 [0.081, 0.583]	1.122 [0.421, 1.980]
Toronto	0.572 [0.347, 0.794]	0.943 [0.464, 1.554]
UCSF	0.498 [0.326, 0.673]	0.812 [0.280, 1.383]
MUSIC	0.441 [0.092, 0.767]	0.029 [-0.552, 0.512]
KCL	0.194 [-0.104, 0.540]	0.840 [-0.087, 1.665]

Appendix B. Risk Predictions for Upgrading

Let us assume a new patient j, for whom we need to estimate the upgrading-risk. Let his current follow-up visit time be v, latest time of biopsy be t, observed vector PSA measurements be $\mathcal{Y}_j(v)$. The combined information from the observed data about the time of upgrading, is given by the following posterior predictive distribution $g(T_j^*)$ of his time T_j^* of upgrading:

$$\begin{aligned} g(T_j^*) &= p\big\{T_j^* \mid T_j^* > t, \mathcal{Y}_j(v), \mathcal{A}_n\big\} \\ &= \int\int p\big(T_j^* \mid T_j^* > t, \boldsymbol{b}_j, \boldsymbol{\theta}\big) p\big\{\boldsymbol{b}_j \mid T_j^* > t, \mathcal{Y}_j(v), \boldsymbol{\theta}\big\} p\big(\boldsymbol{\theta} \mid \mathcal{A}_n\big) \mathrm{d}\boldsymbol{b}_j \mathrm{d}\boldsymbol{\theta}. \end{aligned}$$

The distribution $g(T_j^*)$ depends not only depends on the observed data of the patient $T_j^* > t, \mathcal{Y}_j(v)$, but also depends on the information from the PRIAS dataset $\mathcal{A}_n$. To this the the posterior distribution of random effects $\boldsymbol{b}_j$ and posterior distribution of the vector of all parameters $\boldsymbol{\theta}$ are utilized, respectively. The distribution $g(T_j^*)$ can be estimated as detailed in Rizopoulos et al. [11]. Since, many prostate cancer patients may not obtain upgrading in the current follow-up period of PRIAS, $g(T_j^*)$ can only be estimated for a currently limited follow-up period.

The cause-specific cumulative upgrading-risk can be derived from $g(T_j^*)$ as given in [11]. It is given by:

$$R_j(u \mid t, v) = \Pr\big\{T_j^* > u \mid T_j^* > t, \mathcal{Y}_j(v), \mathcal{A}_n\big\}, \quad u \geq t. \tag{4}$$

The personalized risk profile of the patient (see Panel C, Figure 5) updates as more data is gathered over follow-up visits.

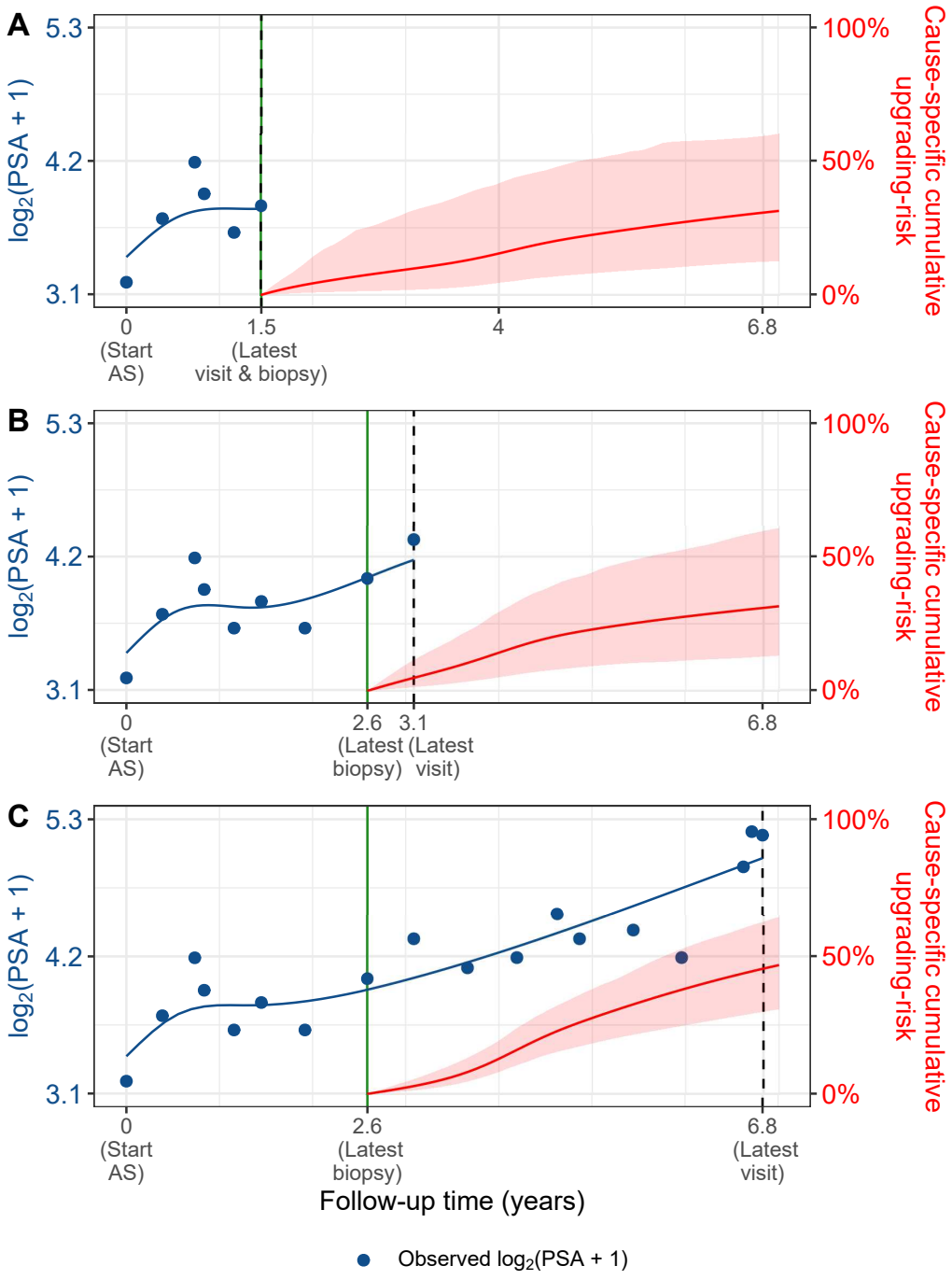

Figure 5: **Cause-specific cumulative upgrading-risk changing dynamically over follow-up** as more patient data is gathered. The three **Panels A,B and C:** are ordered by the time of the latest visit (dashed vertical black line) of a new patient. At each of the latest follow-up visits, we combine the accumulated PSA measurements (shown in blue), and latest time of negative biopsy (solid vertical green line) to obtain the updated cumulative-risk profile (shown in red) of the patient.

Appendix B.1. Validation of Risk Predictions

We wanted to check the usefulness of our model for not only the PRIAS patients but also for patients from other cohorts. To this end, we validated our model in the PRIAS dataset (internal validation) and the largest six cohorts from the GAP3 database [8]. These are the University of Toronto AS (Toronto), Johns Hopkins AS (Hopkins), Memorial Sloan Kettering Cancer Center AS (MSKCC), University of California San Francisco Active Surveillance (UCSF), King's College London AS (KCL), Michigan Urological Surgery Improvement Collaborative AS (MUSIC).

Calibration-in-the-large We first assessed calibration-in-the-large [12] of our model in the aforementioned cohorts. To this end, we used our model to predict the cause-specific cumulative upgrading-risk for each patient, given their PSA measurements and biopsy results. We then averaged the resulting profiles of cause-specific cumulative upgrading-risk. Subsequently, we compared the averaged cumulative-risk profile with a non-parametric estimate [9] of the cause-specific cumulative upgrading-risk in each of the cohorts. The results are shown in Panel A of Figure 6. We can see that our model is miscalibrated in external cohorts, although it is fine in the Hopkins cohort. To improve our model's calibration in all cohorts, we recalibrated the baseline hazard of the joint model fitted to the PRIAS dataset, individually for each of the cohorts except the Hopkins cohort. More specifically, given the data of an external cohort $\mathcal{A}^c$, where c denotes the cohort, the recalibrated parameters $\boldsymbol{\gamma}^c_{h_0}$ (Appendix A) of the log baseline hazard are given by:

$$p(\boldsymbol{\gamma}^c_{h_0} \mid \mathcal{A}^c, \boldsymbol{b^c}, \boldsymbol{\theta}) \propto \prod_{i=1}^{n^c} p(l^c_i, r^c_i \mid \boldsymbol{b^c_i}, \boldsymbol{\theta}) p(\boldsymbol{\gamma}^c_{h_0}) \tag{5}$$

where n^c are the number of patients in the c-th cohort, and $\boldsymbol{\theta}$ is the vector of all parameters of the joint model fitted to the PRIAS dataset. The interval in which upgrading is observed for the i-th patient is given by l^c_i, r^c_i, with $r^c_i = \infty$ for right-censored patients. The symbol $\boldsymbol{b^c_i}$ denotes patient-specific random effects (Appendix A) in the c-th cohort. The random effects are obtained using the joint model fitted to the PRIAS dataset before recalibration. We re-evaluated the calibration-in-the-large of our model after the recalibration of the baseline hazard individually for each cohort. The improved calibration-in-the-large is shown in Panel B of Figure 6.

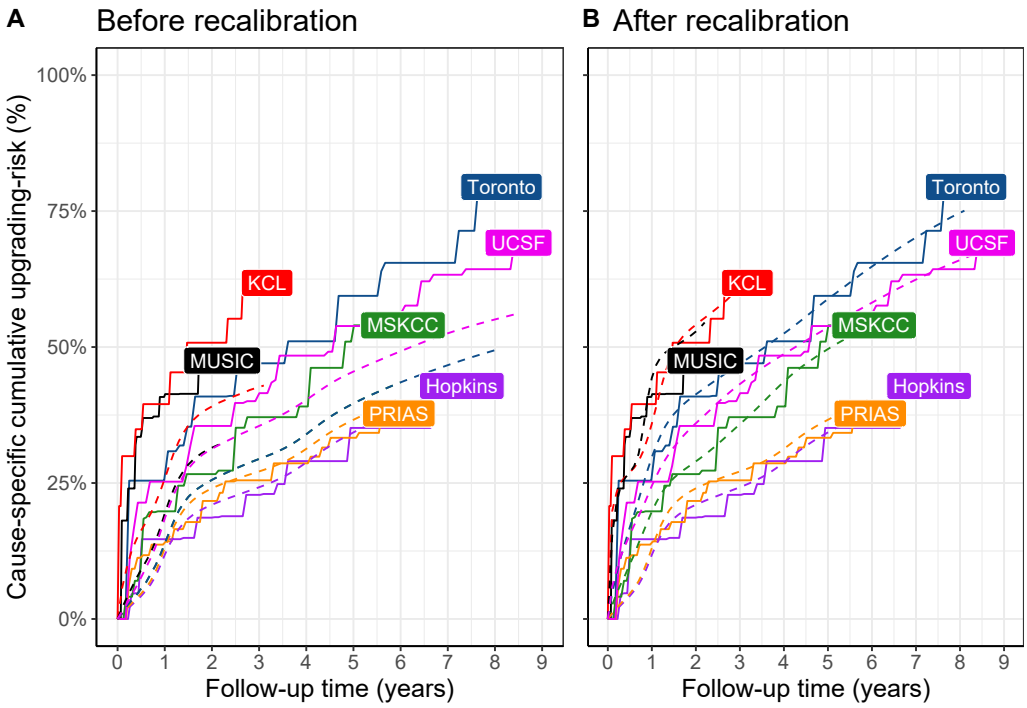

Figure 6: **Calibration-in-the-large of our model:**. In **Panel A** we can see that our model is not well calibrated for use in KCL, MUSIC, Toronto and MSKCC. In **Panel B** we can see that calibration of model predictions improved in KCL, MUSIC, Toronto and MSKCC cohorts after recalibrating our model. Recalibration was not necessary for Hopkins cohort. Full names of Cohorts are *PRIAS*: Prostate Cancer International Active Surveillance, *Toronto*: University of Toronto Active Surveillance, *Hopkins*: Johns Hopkins Active Surveillance, *MSKCC*: Memorial Sloan Kettering Cancer Center Active Surveillance, *KCL*: King's College London Active Surveillance, *MUSIC*: Michigan Urological Surgery Improvement Collaborative Active Surveillance, *UCSF*: University of California San Francisco Active Surveillance.

Recalibrated PRIAS Model Versus Individual Joint Models For Each Cohort We wanted to check if our recalibrated PRIAS model performed as good as a new joint model that could be fitted to the external cohorts. To this end, we predicted cause-specific cumulative upgrading-risk for each patient from each cohort using two sets of models, namely the recalibrated PRIAS model for each cohort, and a new joint model fitted to each cohort. The difference in predicted cause-specific cumulative upgrading-risk from these models is shown in Figure 7. We can see that the difference is smaller in those cohorts in which the effects of $\log_2(\text{PSA} + 1)$ value and velocity were similar to that of PRIAS (Table 8). For example, the Hopkins cohort had parameter estimates similar to that of PRIAS, and consequently, the difference in predicted risks for this cohort is smallest. The opposite of this phenomenon holds for the MUSIC and KCL cohorts.

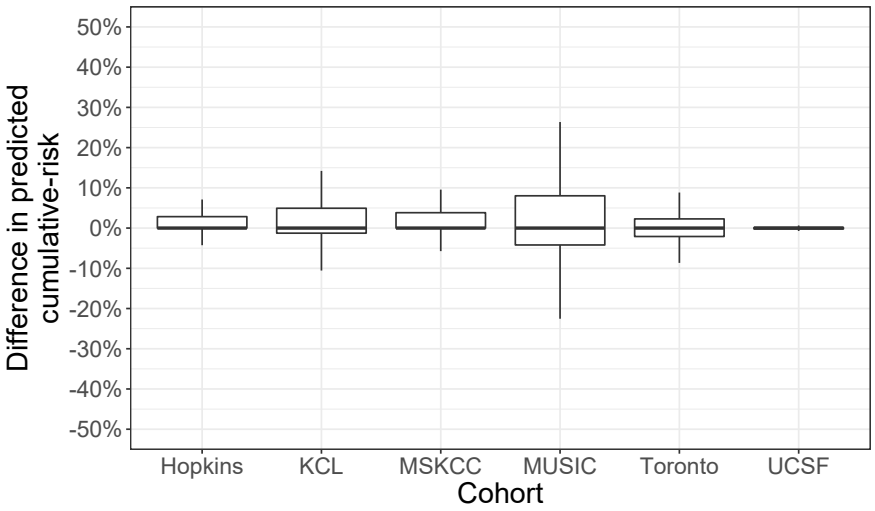

Figure 7: **Comparison of predictions from recalibrated PRIAS model with individual joint models fitted to external cohorts:** On Y-axis we show the difference between predicted cause-specific cumulative upgrading-risk for individual patients using two models, namely the recalibrated PRIAS model for each cohort, and individual joint model fitted to each cohort. The figure shows that the difference is smaller in those cohorts in which the effects of $\log_2(\text{PSA} + 1)$ value and velocity were similar to that of PRIAS (Table 8). Full names of Cohorts are *PRIAS*: Prostate Cancer International Active Surveillance, *Toronto*: University of Toronto Active Surveillance, *Hopkins*: Johns Hopkins Active Surveillance, *MSKCC*: Memorial Sloan Kettering Cancer Center Active Surveillance, *KCL*: King's College London Active Surveillance, *MUSIC*: Michigan Urological Surgery Improvement Collaborative Active Surveillance, *UCSF*: University of California San Francisco Active Surveillance.

Validation of Dynamic Cumulative-Risk Predictions As shown in Figure 5, the cumulative-risk predictions from the joint model are dynamic in nature. That is, they update as more data becomes available over time. Consequently, the discrimination and prediction error of the joint model also depend on the available data. We assessed these two measures dynamically in the PRIAS cohort (interval validation) and in the largest six external cohorts that are part of the GAP3 database. For discrimination, we utilized the time-varying area under the receiver operating characteristic curve or time-varying AUC [11]. For time-varying prediction error, we assessed the mean absolute prediction error or MAPE [11]. The AUC indicates how well the model discriminates between patients who experience upgrading, and those do not. The MAPE indicates how accurately the model predicts upgrading. Both AUC and MAPE are restricted to $[0, 1]$. However, it is preferred that AUC > 0.5 because an AUC ≤ 0.5 indicates that the model performs worse than random discrimination. Ideally, MAPE should be 0.

We calculate AUC and MAPE in a time-dependent manner. More specifically, given the time of latest biopsy t, and history of PSA measurements up to time v, we calculate AUC and MAPE for a medically relevant time frame $(t, v]$, within which the occurrence of upgrading is of interest. In the case of prostate cancer, at any point in time v, it is of interest to identify patients who may have experienced upgrading in the last one year $(v - 1, v]$. That is, we set $t = v - 1$. We then calculate AUC and MAPE at a gap of every six months (follow-up schedule of PRIAS). That is, $v \epsilon \{1, 1.5, \ldots\}$ years. To obtain reliable estimates of AUC and MAPE, in each cohort, we restrict v to a maximum time point $v_{\max}$, such that there are at least ten patients who experience upgrading after $v_{\max}$. This maximum time point $v_{\max}$ differs between cohorts, and is given in Table 9.

The results for estimates of AUC and MAPE are summarized in Figure 8, and in Table 10 to Table 16. Results are based on the recalibrated PRIAS model for the GAP3 cohorts. The results show that AUC remains more or less constant in all cohorts as more data becomes available for patients. The AUC obtains a moderate value, roughly between 0.5 and 0.7 for all cohorts. On the other hand, MAPE reduces by a big margin after year one of follow-up. This could be because of two reasons. Firstly, MAPE at year one is based only on four PSA measurements gathered in the first year of follow-up, whereas after year one number of PSA measurements increases. Secondly, patients in year one consist of two sub-populations, namely patients with a correct Gleason grade group 1 at the time of inclusion in AS, and patients

Table 9: **Maximum follow-up period up to which we can reliably predict upgrading-risk**. In each cohort, this time point is chosen such that there are at least 10 patients who experience upgrading after this time point. Full names of Cohorts are *PRIAS*: Prostate Cancer International Active Surveillance, *Toronto*: University of Toronto Active Surveillance, *Hopkins*: Johns Hopkins Active Surveillance, *MSKCC*: Memorial Sloan Kettering Cancer Center Active Surveillance, *KCL*: King's College London Active Surveillance, *MUSIC*: Michigan Urological Surgery Improvement Collaborative Active Surveillance, *UCSF*: University of California San Francisco Active Surveillance.

Cohort	Maximum Prediction Time (years)
PRIAS	6
KCL	3
MUSIC	2
Toronto	8
MSKCC	6
Hopkins	7
UCSF	8.5

who probably had Gleason grade group 2 at inclusion but were misclassified by the urologist as Gleason grade group 1 patients. To remedy this problem, a biopsy for all patients at year one is commonly recommended in all AS programs [13].

Table 10: **Internal validation of predictions of upgrading in PRIAS cohort**. The area under the receiver operating characteristic curve or AUC (measure of discrimination) and mean absolute prediction error or MAPE are calculated over the follow-up period at a gap of 6 months. In addition bootstrapped 95% confidence intervals (CI) are also presented.

Follow-up period (years)	AUC (95% CI)	MAPE (95%CI)
1.0 to 2.0	0.661 [0.647, 0.678]	0.187 [0.183, 0.191]
1.5 to 2.5	0.647 [0.596, 0.688]	0.129 [0.122, 0.140]
2.0 to 3.0	0.683 [0.642, 0.723]	0.135 [0.125, 0.146]
2.5 to 3.5	0.692 [0.632, 0.748]	0.118 [0.111, 0.128]
3.0 to 4.0	0.657 [0.603, 0.709]	0.086 [0.080, 0.092]
3.5 to 4.5	0.623 [0.582, 0.660]	0.111 [0.105, 0.116]
4.0 to 5.0	0.619 [0.582, 0.654]	0.126 [0.118, 0.131]
4.5 to 5.5	0.624 [0.537, 0.711]	0.119 [0.103, 0.135]
5.0 to 6.0	0.639 [0.582, 0.696]	0.121 [0.103, 0.138]

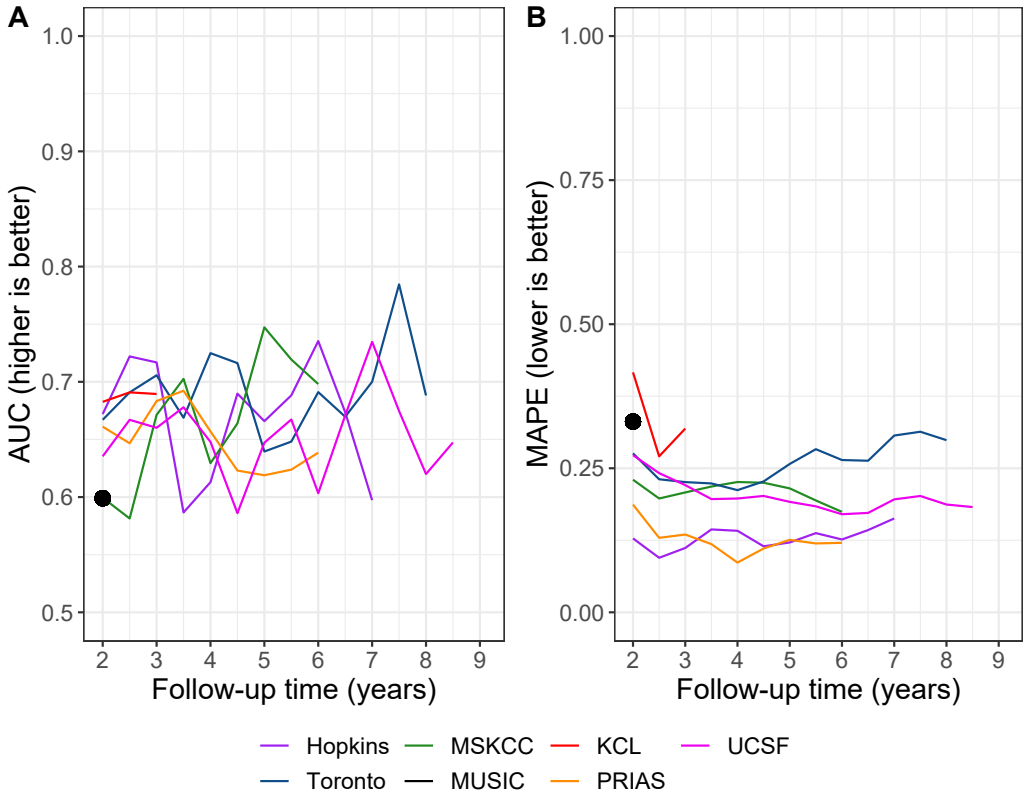

Figure 8: **Validation of dynamic predictions of cause-specific cumulative upgrading-risk**. In **Panel A** area under the receiver operating characteristic curve or AUC (measure of discrimination) is between 0.6 and 0.7. **Panel B** we can see that the time dependent root mean squared prediction error or MAPE is similar for PRIAS and Hopkins cohorts. The bootstrapped 95% confidence interval for these estimates are presented in Table 10 to Table 15. Full names of Cohorts are *PRIAS*: Prostate Cancer International Active Surveillance, *Toronto*: University of Toronto Active Surveillance, *Hopkins*: Johns Hopkins Active Surveillance, *MSKCC*: Memorial Sloan Kettering Cancer Center Active Surveillance, *KCL*: King's College London Active Surveillance, *MUSIC*: Michigan Urological Surgery Improvement Collaborative Active Surveillance, *UCSF*: University of California San Francisco Active Surveillance.

Table 11: **External validation of predictions of upgrading in University of Toronto Active Surveillance cohort**. The area under the receiver operating characteristic curve or AUC (measure of discrimination) and mean absolute prediction error or MAPE are calculated over the follow-up period at a gap of 6 months. In addition bootstrapped 95% confidence intervals (CI) are also presented.

Follow-up period (years)	AUC (95% CI)	MAPE (95%CI)
1.0 to 2.0	0.667 [0.634, 0.712]	0.276 [0.259, 0.296]
1.5 to 2.5	0.691 [0.651, 0.730]	0.231 [0.205, 0.254]
2.0 to 3.0	0.706 [0.637, 0.762]	0.226 [0.196, 0.260]
2.5 to 3.5	0.669 [0.586, 0.741]	0.224 [0.195, 0.258]
3.0 to 4.0	0.725 [0.649, 0.806]	0.212 [0.184, 0.238]
3.5 to 4.5	0.716 [0.642, 0.793]	0.227 [0.206, 0.258]
4.0 to 5.0	0.640 [0.579, 0.717]	0.257 [0.222, 0.312]
4.5 to 5.5	0.648 [0.579, 0.740]	0.283 [0.247, 0.326]
5.0 to 6.0	0.691 [0.608, 0.793]	0.264 [0.232, 0.302]
5.5 to 6.5	0.670 [0.543, 0.776]	0.263 [0.227, 0.307]
6.0 to 7.0	0.700 [0.544, 0.851]	0.307 [0.258, 0.363]
6.5 to 7.5	0.785 [0.640, 0.866]	0.313 [0.272, 0.360]
7.0 to 8.0	0.688 [0.532, 0.786]	0.299 [0.249, 0.361]

Table 12: **External validation of predictions of upgrading in University of California San Francisco Active Surveillance cohort**. The area under the receiver operating characteristic curve or AUC (measure of discrimination) and mean absolute prediction error or MAPE are calculated over the follow-up period at a gap of 6 months. In addition bootstrapped 95% confidence intervals (CI) are also presented.

Follow-up period (years)	AUC (95% CI)	MAPE (95%CI)
1.0 to 2.0	0.635 [0.595, 0.677]	0.273 [0.266, 0.281]
1.5 to 2.5	0.667 [0.628, 0.715]	0.241 [0.224, 0.259]
2.0 to 3.0	0.660 [0.600, 0.713]	0.221 [0.205, 0.238]
2.5 to 3.5	0.678 [0.614, 0.757]	0.197 [0.175, 0.214]
3.0 to 4.0	0.648 [0.574, 0.707]	0.197 [0.179, 0.221]
3.5 to 4.5	0.586 [0.525, 0.638]	0.202 [0.180, 0.229]
4.0 to 5.0	0.647 [0.590, 0.754]	0.192 [0.168, 0.217]
4.5 to 5.5	0.667 [0.582, 0.773]	0.184 [0.159, 0.220]
5.0 to 6.0	0.603 [0.496, 0.696]	0.170 [0.144, 0.207]
5.5 to 6.5	0.671 [0.576, 0.786]	0.173 [0.145, 0.202]
6.0 to 7.0	0.735 [0.663, 0.794]	0.196 [0.166, 0.219]
6.5 to 7.5	0.675 [0.565, 0.769]	0.202 [0.168, 0.231]
7.0 to 8.0	0.620 [0.518, 0.740]	0.187 [0.144, 0.217]
7.5 to 8.5	0.647 [0.538, 0.787]	0.183 [0.146, 0.222]

Table 13: **External validation of predictions of upgrading in Johns Hopkins Active Surveillance cohort**. The area under the receiver operating characteristic curve or AUC (measure of discrimination) and mean absolute prediction error or MAPE are calculated over the follow-up period at a gap of 6 months. In addition bootstrapped 95% confidence intervals (CI) are also presented.

Follow-up period (years)	AUC (95% CI)	MAPE (95%CI)
1.0 to 2.0	0.672 [0.604, 0.744]	0.128 [0.115, 0.141]
1.5 to 2.5	0.722 [0.652, 0.792]	0.095 [0.081, 0.111]
2.0 to 3.0	0.717 [0.638, 0.777]	0.112 [0.100, 0.123]
2.5 to 3.5	0.587 [0.493, 0.704]	0.144 [0.129, 0.154]
3.0 to 4.0	0.613 [0.486, 0.742]	0.141 [0.126, 0.156]
3.5 to 4.5	0.690 [0.594, 0.783]	0.115 [0.100, 0.133]
4.0 to 5.0	0.666 [0.572, 0.754]	0.121 [0.104, 0.147]
4.5 to 5.5	0.688 [0.519, 0.779]	0.137 [0.119, 0.161]
5.0 to 6.0	0.735 [0.676, 0.820]	0.126 [0.102, 0.152]
5.5 to 6.5	0.674 [0.581, 0.765]	0.143 [0.121, 0.172]
6.0 to 7.0	0.597 [0.472, 0.712]	0.163 [0.126, 0.195]

Table 14: **External validation of predictions of upgrading in Memorial Sloan Kettering Cancer Center Active Surveillance cohort**. The area under the receiver operating characteristic curve or AUC (measure of discrimination) and mean absolute prediction error or MAPE are calculated over the follow-up period at a gap of 6 months. In addition bootstrapped 95% confidence intervals (CI) are also presented.

Follow-up period (years)	AUC (95% CI)	MAPE (95%CI)
1.0 to 2.0	0.599 [0.518, 0.671]	0.230 [0.207, 0.256]
1.5 to 2.5	0.581 [0.504, 0.663]	0.198 [0.168, 0.235]
2.0 to 3.0	0.671 [0.599, 0.741]	0.208 [0.182, 0.232]
2.5 to 3.5	0.703 [0.610, 0.777]	0.218 [0.197, 0.246]
3.0 to 4.0	0.629 [0.499, 0.706]	0.226 [0.194, 0.259]
3.5 to 4.5	0.664 [0.589, 0.756]	0.225 [0.199, 0.262]
4.0 to 5.0	0.747 [0.642, 0.841]	0.215 [0.188, 0.247]
4.5 to 5.5	0.719 [0.597, 0.852]	0.194 [0.165, 0.232]
5.0 to 6.0	0.698 [0.565, 0.792]	0.174 [0.136, 0.227]

Table 15: **External validation of predictions of upgrading in King's College London Active Surveillance cohort**. The area under the receiver operating characteristic curve or AUC (measure of discrimination) and mean absolute prediction error or MAPE are calculated over the follow-up period at a gap of 6 months. In addition bootstrapped 95% confidence intervals (CI) are also presented.

Follow-up period (years)	AUC (95% CI)	MAPE (95%CI)
1.0 to 2.0	0.683 [0.604, 0.753]	0.416 [0.396, 0.445]
1.5 to 2.5	0.691 [0.621, 0.766]	0.271 [0.246, 0.297]
2.0 to 3.0	0.689 [0.616, 0.785]	0.319 [0.282, 0.344]

Table 16: **External validation of predictions of upgrading in Michigan Urological Surgery Improvement Collaborative Active Surveillance cohort**. The area under the receiver operating characteristic curve or AUC (measure of discrimination) and mean absolute prediction error or MAPE are calculated over the follow-up period at a gap of 6 months. In addition bootstrapped 95% confidence intervals (CI) are also presented.

Follow-up period (years)	AUC (95% CI)	MAPE (95%CI)
1.0 to 2.0	0.599 [0.553, 0.632]	0.331 [0.317, 0.348]

Appendix C. Personalized Biopsies Based on Cause-Specific Cumulative Upgrading-Risk

Consider some real patients from the PRIAS database shown in Figure 10– 12. In line with the protocols of most AS cohorts [14], we first schedule a compulsory biopsy at year one of follow-up. This promises early detection of Gleason upgrade for patients misdiagnosed as low-grade cancer patients or patients who chose AS despite having a higher grade at diagnosis. We also maintain a recommended minimum gap of one year between consecutive biopsies [13]. That is, we intend to develop a personalized schedule of biopsies for these patients starting from the second year. The added benefit of planning biopsies year two onwards is that due to the longitudinal measurements accumulated over two years, and year one biopsy results, we are able to make reasonably accurate predictions of the cause-specific cumulative upgrading-risk.

Using the joint model fitted to the PRIAS dataset, we first obtain a patient's cause-specific cumulative upgrading-risk over the entire future follow-up period (see 4), given their accumulated two year clinical data. Typically biopsies may be decided on the same visit on which PSA is measured. Let $U = u_1, \ldots, u_L$ represent a schedule of such visits (e.g., every six months in prostate cancer for PSA measurement), where $u_1 = v$ is also the time of the current visit, and u_L is the horizon up to which we intend to plan biopsies. Depending upon how much training/validation data is available, this horizon differs between cohorts (Table 17). First, we make L successive decisions for conducting biopsies on each of the L future visit times $u_l \in U$. Specifically, we decide to conduct a biopsy at time u_l if the conditional cumulative-risk of upgrading at u_l is larger than a certain risk threshold $0 \leq \kappa \leq 1$ (e.g., $\kappa = 12\%$ risk as shown in Figure 9). If a biopsy gets planned at time u_l, then the successive biopsy decision at time u_{l+1} is made using an updated cumulative-risk profile. This updated cumulative-risk profile accounts for the possibility that upgrading may occur after time $u_l < T_j^*$. The biopsy decisions on each future visit time u_l are defined as:

$$Q_j^{\kappa}(u_l \mid t_l, v) = I\big\{R_j(u_l \mid t_l, v) \geq \kappa\big\},$$

$$t_l = \left\{ \begin{array}{lll} t, & \text{if} & l = 1 \\ t_{l-1}, & \text{if} & Q_j^{\kappa}(u_{l-1} \mid t_{l-1}, v) = 0, l \geq 2 \\ u_{l-1}, & \text{if} & Q_j^{\kappa}(u_{l-1} \mid t_{l-1}, v) = 1, l \geq 2 \end{array} \right\}.$$

The cumulative-risk $R_j(u_l \mid t_l, v)$ at future visit time u_l utilizes the time t_l

as the time of the last conducted biopsy on which upgrading may not be observed. However, the contribution of the observed longitudinal data $\mathcal{Y}_j(v)$ in the risk function remains the same over all time points in U. The biopsy decision at time u_l is denoted by $Q_j^\kappa(u_l \mid t_l, v)$. Via the indicator function $I(\cdot)$ it obtains a value 1 (or 0) when a biopsy is to be conducted (or not conducted) at time u_l. The subset of future time points in U on which a biopsy is to be performed results into a personalized schedule of planned future biopsies, given by:

$$S_j^\kappa(U \mid t, v) = \big\{u_l \in U \mid Q_j^\kappa(u_l \mid t_l, v) = 1\big\}. \tag{6}$$

The personalized schedule in (6) is updated as more patient data becomes available over subsequent follow-up visits.

Appendix C.1. Expected Time Delay in Detecting Upgrading

The schedule $S_j^\kappa(U \mid t, v)$ manifests a personalized biopsy plan for the j-the patient. However, the time delay in detecting upgrading that may subsequently be observed depends on the true time of upgrading T_j^* of the patient. Since two different patients with the same timing of biopsies will expect different time delays, we estimate it in a patient-specific manner as well. Although, this calculation is not limited to personalized schedules only, but can be done for any schedule S of biopsies with N time points $S = \{s_n \mid n = 1, \ldots, N\}$.

For each of the N planned biopsies there exist N possible time intervals $s_{n-1} < T_j^* \leq s_n$ in which upgrading may be observed. Correspondingly, there are N possible time delays in detecting upgrading $s_n - T_j^*$. Given a schedule S, the true time delay in detecting upgrading D_j that the patient will experience can be defined as:

$$D_j(S \mid t) = \left\{ \begin{array}{ll} s_1 - T_j^*, & \text{if} \quad t < T_j^* \leq s_1 \\ \ldots & \\ s_N - T_j^*, & \text{if} \quad s_{N-1} < T_j^* \leq s_N \end{array} \right\}. \tag{7}$$

The time delay is cannot be defined for the scenario in which the patient obtains upgrading after the time of the last biopsy in the schedule $T_j^* > s_N$. Hence, this delay should be interpreted as the delay that will be observed if the patient will experience upgrading before time of the last planned biopsy at $T_j^* \leq s_N$. To estimate the expected value of $D_j(\cdot)$ in a patient-specific manner, we exploit the personalized cumulative-risk profile of the patient

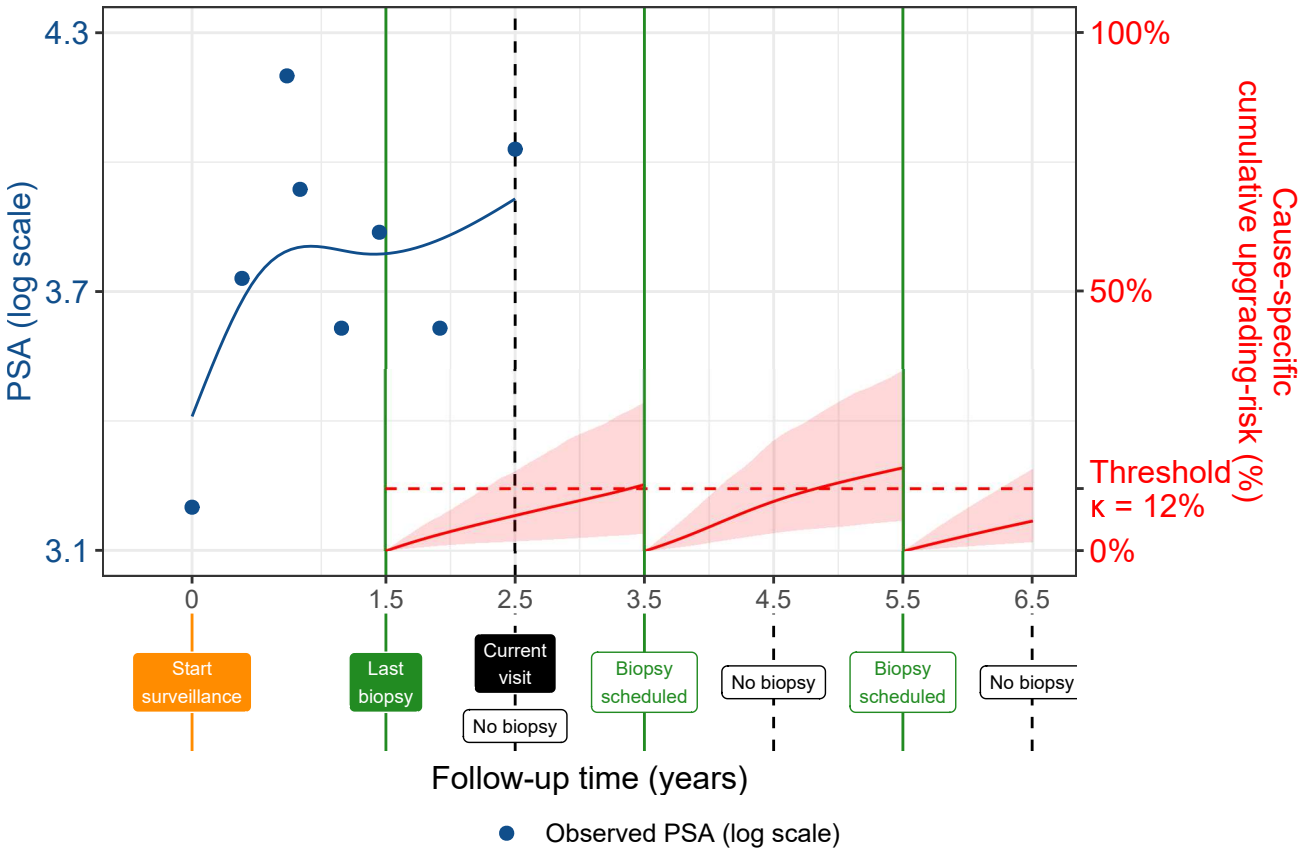

Figure 9: **Illustration of Personalized Biopsy Decisions Using Patient-specific Conditional Cumulative Upgrading-risk**. The last biopsy on which upgrading was not observed was conducted at $t = 1.5$ years. The current visit time of the patient is $v = 2.5$ years. Decisions for biopsy need to be made at a gap of every one year starting from the current visit until a horizon of 6.5 years. That is, $U = \{2.5, 3.5, 4.5, 5.5, 6.5\}$ years. Based on an example risk threshold of 12% ($\kappa = 0.12$) the future biopsy decisions at time points in U lead to a personalized schedule $S_j^{\kappa^*}(U \mid t = 1.5, v = 2.5) = \{3.5, 5.5\}$ years. The conditional cumulative-risk profiles $R_j(u_l \mid t_l, v)$ employed in (Appendix C) are shown with red line (confidence interval shaded). It is called 'conditional' because, for example, the second biopsy at future time 5.5 years, is scheduled after accounting for the possibility that upgrading (true time T_j^*) may not have occurred until the time of the previously scheduled biopsy at time $T_j^* > 3.5$ years. All values are illustrative.

defined in (4). Specifically, the expected time delay $E\{D_j(\cdot)\}$ can be calculated as the weighted sum of N possible time delays defined in (7). The n-th weight is equal to the probability of the patient obtaining upgrading in the n-th interval $s_{n-1} < T_j^* \leq s_n$.

$$E\Big\{D_j(S \mid t)\Big\} = \sum_{n=1}^{N} \Big\{s_n - E(T_j^* \mid s_{n-1}, s_n, v)\Big\} \times \Pr\Big\{s_{n-1} < T_j^* \leq s_n \mid T_j^* \leq s_N, \mathcal{Y}_j(v), \mathcal{A}_n\Big\}, \quad s_0 = t$$

$$E(T_j^* \mid s_{n-1}, s_n, v) = s_{n-1} + \int_{s_{n-1}}^{s_n} \Pr\Big\{T_j^* \geq u \mid s_{n-1} < T_j^* \leq s_n, \mathcal{Y}_j(v), \mathcal{A}_n\Big\} \mathrm{d}u,$$

where $E(T_j^* \mid s_{n-1}, s_n, v)$ denotes the conditional expected time of upgrading for the scenario $s_{n-1} < T_j^* \leq s_n$, and is calculated as the area under the corresponding survival curve.

The personalized expected time delay in detecting upgrading has the advantage that it is updated over follow-up as more patient data become available. Since it can be calculated for any schedule, patients and doctors can utilize it along with the plan of biopsies to compare schedules before making a decision. Although, in order to have a fair comparison of time delays between different schedules for the same patient, a compulsory biopsy at a common horizon time point should be planned in all schedules.

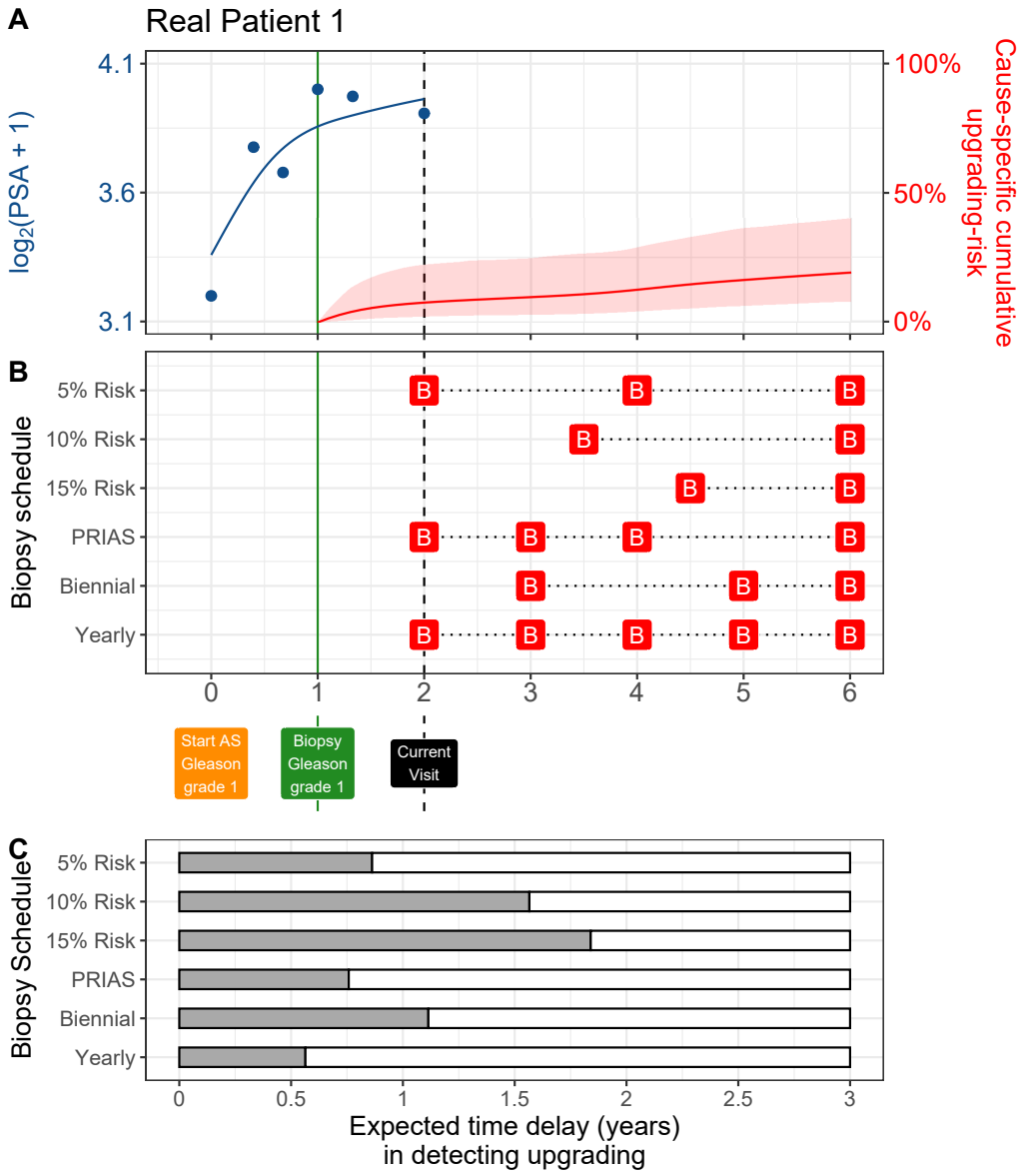

Figure 10: **Personalized and fixed schedules of biopsies for patient 1**. **Panel A:** shows the observed and fitted $\log_2(\text{PSA} + 1)$ measurements (Equation 1), and the dynamic cause-specific cumulative upgrading-risk (see Appendix B) over follow-up period. **Panel B** shows the personalized and fixed schedules of biopsies with a 'B' indicating times of biopsies. Smaller risk thresholds lead to more frequently planned biopsies. **Panel C** various schedules are compared in terms of the expected time delay in detecting upgrading (years) if patient progresses before year six. The maximum time delay with limited adverse consequences is three years [15]. A compulsory biopsy was scheduled at year six (maximum biopsy scheduling time in PRIAS, Table 17) in all schedules for a meaningful comparison between them.

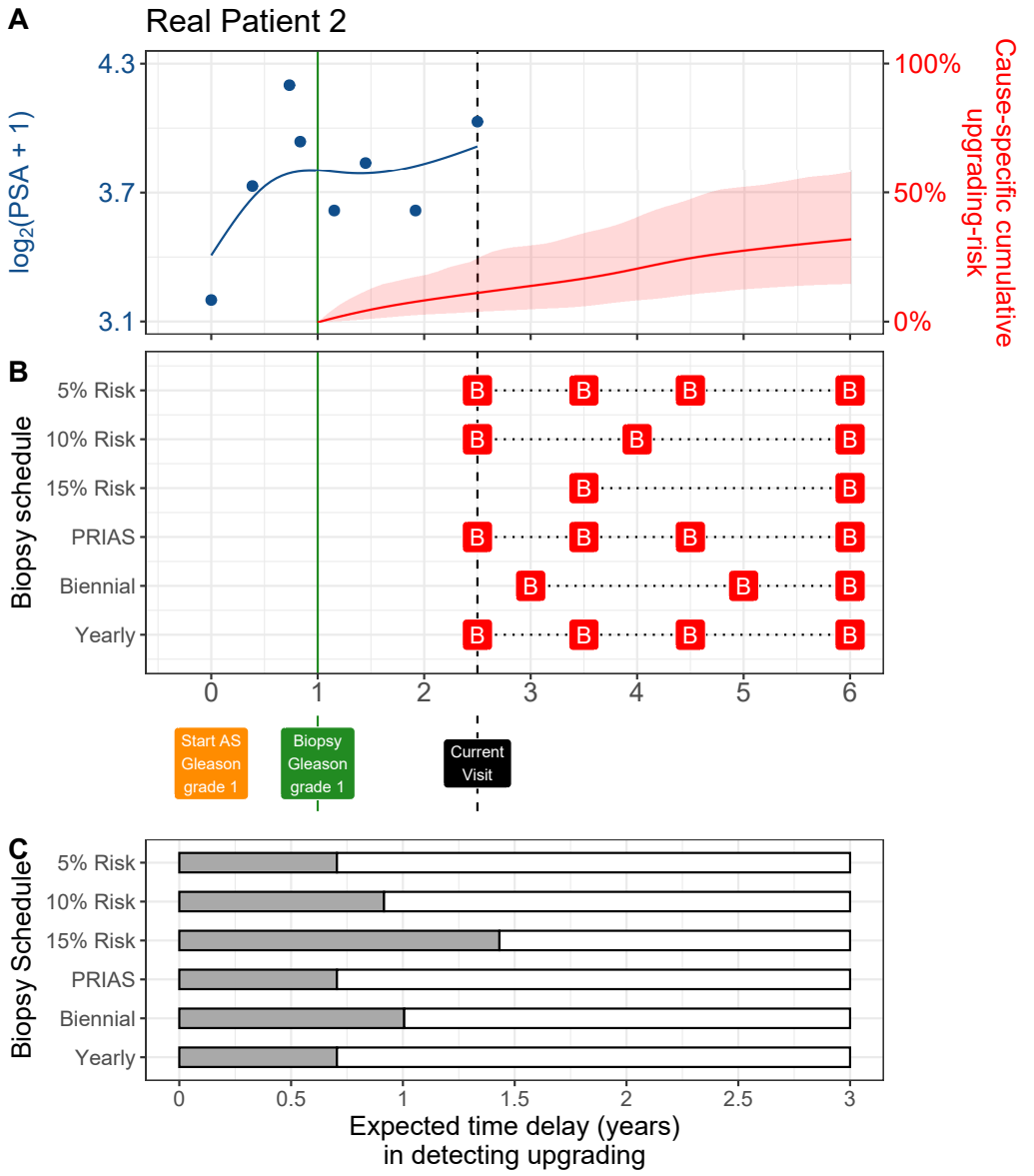

Figure 11: **Personalized and fixed schedules of biopsies for patient 2**. **Panel A:** shows the observed and fitted $\log_2(\text{PSA} + 1)$ measurements (Equation 1), and the dynamic cause-specific cumulative upgrading-risk (see Appendix B) over follow-up period. **Panel B** shows the personalized and fixed schedules of biopsies with a 'B' indicating times of biopsies. Smaller risk thresholds lead to more frequently planned biopsies. **Panel C** various schedules are compared in terms of the expected time delay in detecting upgrading (years) if patient progresses before year six. The maximum time delay with limited adverse consequences is three years [15]. A compulsory biopsy was scheduled at year six (maximum biopsy scheduling time in PRIAS, Table 17) in all schedules for a meaningful comparison between them.

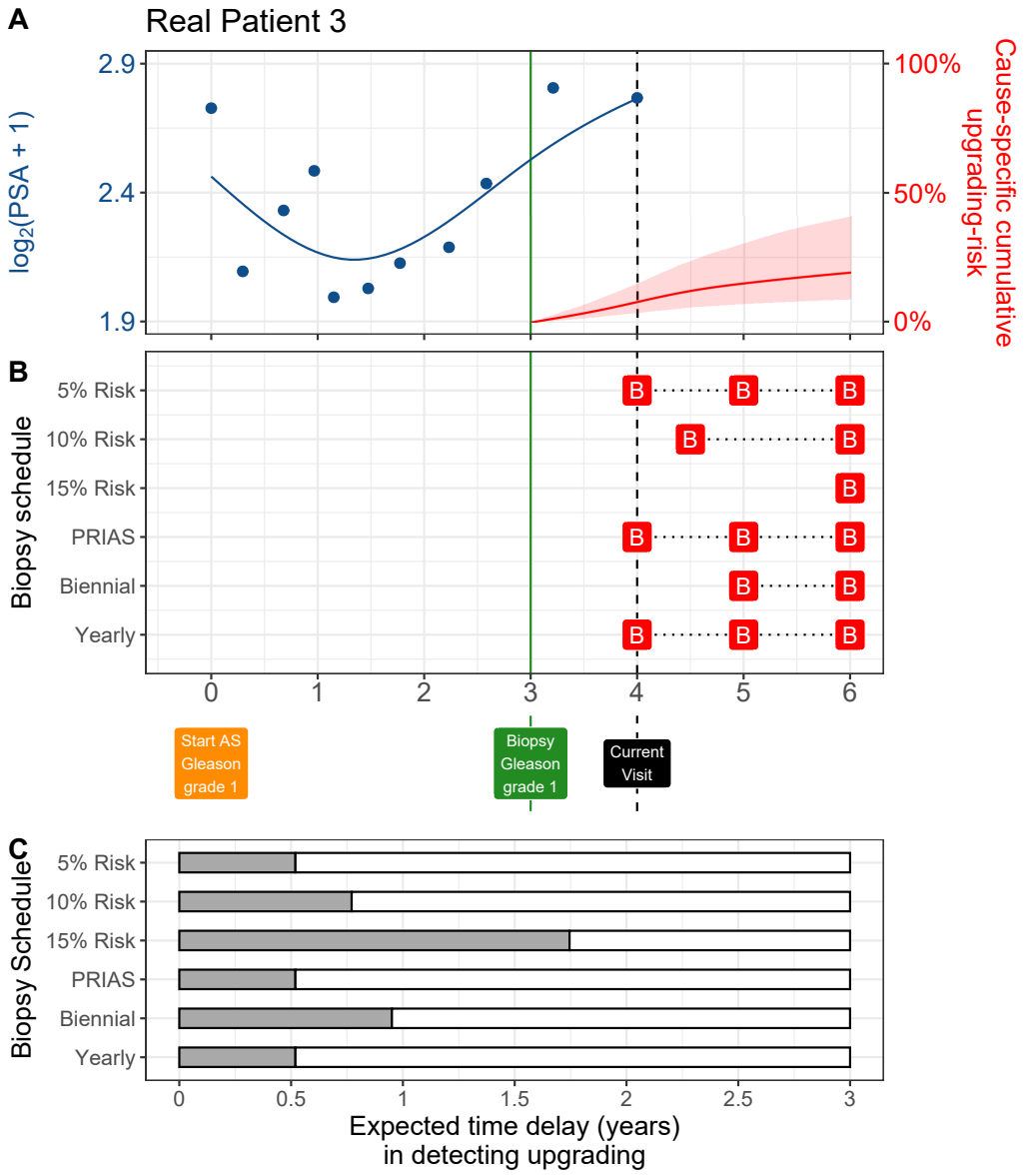

Figure 12: **Personalized and fixed schedules of biopsies for patient 3**. **Panel A:** shows the observed and fitted $\log_2(\text{PSA} + 1)$ measurements (Equation 1), and the dynamic cause-specific cumulative upgrading-risk (see Appendix B) over follow-up period. **Panel B** shows the personalized and fixed schedules of biopsies with a 'B' indicating times of biopsies. Smaller risk thresholds lead to more frequently planned biopsies. **Panel C** various schedules are compared in terms of the expected time delay in detecting upgrading (years) if patient progresses before year six. The maximum time delay with limited adverse consequences is three years [15]. A compulsory biopsy was scheduled at year six (maximum biopsy scheduling time in PRIAS, Table 17) in all schedules for a meaningful comparison between them.

Table 17: **Maximum follow-up period up to which we can reliably make personalized schedules**. In each cohort, this time point is chosen such that there are at least 10 patients who experience upgrading after this time point. Full names of Cohorts are *PRIAS*: Prostate Cancer International Active Surveillance, *Toronto*: University of Toronto Active Surveillance, *Hopkins*: Johns Hopkins Active Surveillance, *MSKCC*: Memorial Sloan Kettering Cancer Center Active Surveillance, *KCL*: King's College London Active Surveillance, *MUSIC*: Michigan Urological Surgery Improvement Collaborative Active Surveillance, *UCSF*: University of California San Francisco Active Surveillance.

Cohort	Maximum Personalized Schedule Time (years)
PRIAS	6
KCL	3
MUSIC	2
Toronto	8
MSKCC	6
Hopkins	7
UCSF	8.5

Appendix D. Web-Application for Practical Use of Personalized Schedule of Biopsies

We implemented our methodology in a web-application to assist patients and doctors in better decision making. It works on desktop as well as mobile devices. The cohorts that are currently supported in this web-application are PRIAS and the largest six cohorts from the GAP3 database [8]. These are the University of Toronto AS (Toronto), Johns Hopkins AS (Hopkins), Memorial Sloan Kettering Cancer Center AS (MSKCC), King's College London AS (KCL), Michigan Urological Surgery Improvement Collaborative AS (MUSIC), and University of California San Francisco Active Surveillance (UCSF). The web application is hosted at `https://emcbiostatistics.shinyapps.io/prias_biopsy_recommender/`.

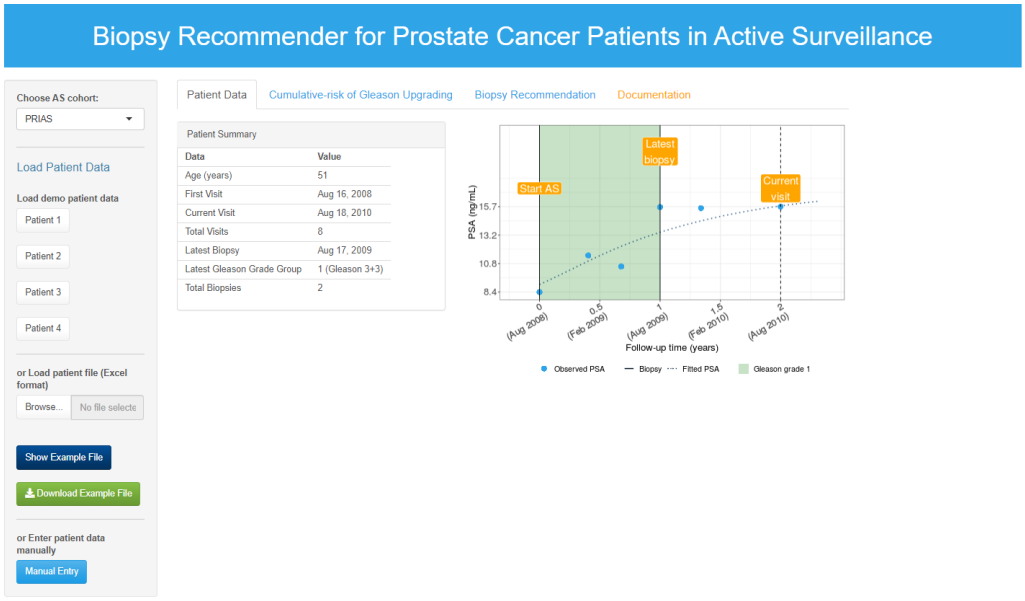

Figure 13: Landing page of the web-application. Panel on the left allows users to load patient data and panel on the right provides information. Patient data can be entered manually, or via Excel files. In addition, demo patient data is already uploaded to assist users in understanding the web-application.

Appendix E. Source Code

The R code for fitting the joint model to the PRIAS dataset, is at `https://github.com/anirudhtomer/prias/tree/master/src/clinical_gap3`. We refer to this location as 'R_HOME' in the rest of this document.

Appendix E.1. Fitting the Joint Model to the PRIAS dataset

Accessing the dataset: The PRIAS dataset is not openly accessible. However, access to the database can be requested via the contact links at `https://www.prias-project.org`.

Formatting the dataset: This dataset, however, is in the so-called wide format and also requires the removal of incorrect entries. This can be done via the R script `R_HOME/dataset_cleaning.R`. This will lead to two R objects, namely 'prias_final.id' and 'prias_long_final'. The 'prias_final.id' object contains information about the time of upgrading for PRIAS patients. The 'prias_long_final' object contains longitudinal PSA measurements, the time of biopsies and results of biopsies.

Fitting the joint model: We use a joint model for time-to-event and longitudinal data to model the evolution of PSA measurements over time, and to simultaneously model their association with the risk of upgrading. The R package we use for this purpose is called **JMbayes** (https://cran.r-project.org/web/packages/JMbayes/JMbayes.pdf). The API we use, however, is currently not hosted on CRAN, and can be found here: `https://github.com/anirudhtomer/JMbayes`. The joint model can be fitted via the script `R_HOME/analysis.R`. It takes roughly 6 hours to run on an Intel Core-i5 machine with four cores and 8GB of RAM.

The graphs presented in the main manuscript, and the supplementary material can be generated by the scripts in `R_HOME/plots/`.

Appendix E.2. Validation of Predictions of Upgrading

Validations can be done using the scripts `R_HOME/validation/auc_brier/auc_calculator.R`, and `R_HOME/validation/auc_brier/gof_calculator.R`. For external validation access to GAP3 database is required.

Appendix E.3. Creating Personalized Schedules of Biopsies

Once a joint model is fitted to the PRIAS dataset, personalized schedules of biopsies based on the risk of upgrading for new patients can be developed as shown in the script `R_HOME/plots/demo_schedule_supplementary.R` or directly using the script `https://raw.githubusercontent.com/anirudhtomer/prias/master/src/lastpaper/pers_schedule_api.R`.

Appendix E.4. Source Code for Web Application

Source code for the shiny web application which provides biopsy schedules for patients can be found at `R_HOME/shinyapp`

Appendix F. Appendix A. Members of The Movember Foundation's Global Action Plan Prostate Cancer Active Surveillance (GAP3) consortium

Principle Investigators: Bruce Trock (Johns Hopkins University, The James Buchanan Brady Urological Institute, Baltimore, USA), Behfar Ehdaie (Memorial Sloan Kettering Cancer Center, New York, USA), Peter Carroll (University of California San Francisco, San Francisco, USA), Christopher Filson (Emory University School of Medicine, Winship Cancer Institute, Atlanta, USA), Jeri Kim / Christopher Logothetis (MD Anderson Cancer Centre, Houston, USA), Todd Morgan (University of Michigan and Michigan Urological Surgery Improvement Collaborative (MUSIC), Michigan, USA), Laurence Klotz (University of Toronto, Sunnybrook Health Sciences Centre, Toronto, Ontario, Canada), Tom Pickles (University of British Columbia, BC Cancer Agency, Vancouver, Canada), Eric Hyndman (University of Calgary, Southern Alberta Institute of Urology, Calgary, Canada), Caroline Moore (University College London & University College London Hospital Trust, London, UK), Vincent Gnanapragasam (University of Cambridge & Cambridge University Hospitals NHS Foundation Trust, Cambridge, UK), Mieke Van Hemelrijck (King's College London, London, UK & Guy's and St Thomas' NHS Foundation Trust, London, UK), Prokar Dasgupta (Guy's and St Thomas' NHS Foundation Trust, London, UK), Chris Bangma (Erasmus Medical Center, Rotterdam, The Netherlands/ representative of Prostate cancer Research International Active Surveillance (PRIAS) consortium), Monique Roobol (Erasmus Medical Center, Rotterdam, The Netherlands/ representative of Prostate cancer Research International Active Surveillance (PRIAS) consortium), The PRIAS study group, Arnauld Villers (Lille University Hospital Center, Lille, France), Antti Rannikko (Helsinki University and Helsinki University Hospital, Helsinki, Finland), Riccardo Valdagni (Department of Oncology and Hemato-oncology, Università degli Studi di Milano, Radiation Oncology 1 and Prostate Cancer Program, Fondazione IRCCS Istituto Nazionale dei Tumori, Milan, Italy), Antoinette Perry (University College Dublin, Dublin, Ireland), Jonas Hugosson (Sahlgrenska University Hospital, Göteborg, Sweden), Jose Rubio-Briones (Instituto Valenciano de Oncología, Valencia, Spain), Anders Bjartell (Skåne University Hospital, Malmö, Sweden), Lukas Hefermehl (Kantonsspital Baden, Baden, Switzerland), Lee Lui Shiong (Singapore General Hospital, Singapore, Singapore), Mark Frydenberg (Monash Health; Monash University,

Melbourne, Australia), Yoshiyuki Kakehi / Mikio Sugimoto (Kagawa University Faculty of Medicine, Kagawa, Japan), Byung Ha Chung (Gangnam Severance Hospital, Yonsei University Health System, Seoul, Republic of Korea)

Pathologist: Theo van der Kwast (Princess Margaret Cancer Centre, Toronto, Canada). Technology Research Partners: Henk Obbink (Royal Philips, Eindhoven, the Netherlands), Wim van der Linden (Royal Philips, Eindhoven, the Netherlands), Tim Hulsen (Royal Philips, Eindhoven, the Netherlands), Cees de Jonge (Royal Philips, Eindhoven, the Netherlands).

Advisory Regional statisticians: Mike Kattan (Cleveland Clinic, Cleveland, Ohio, USA), Ji Xinge (Cleveland Clinic, Cleveland, Ohio, USA), Kenneth Muir (University of Manchester, Manchester, UK), Artitaya Lophatananon (University of Manchester, Manchester, UK), Michael Fahey (Epworth HealthCare, Melbourne, Australia), Ewout Steyerberg (Erasmus Medical Center, Rotterdam, The Netherlands), Daan Nieboer (Erasmus Medical Center, Rotterdam, The Netherlands); Liying Zhang (University of Toronto, Sunnybrook Health Sciences Centre, Toronto, Ontario, Canada)

Executive Regional statisticians: Ewout Steyerberg (Erasmus Medical Center, Rotterdam, The Netherlands), Daan Nieboer (Erasmus Medical Center, Rotterdam, The Netherlands); Kerri Beckmann (King's College London, London, UK & Guy's and St Thomas' NHS Foundation Trust, London, UK), Brian Denton (University of Michigan, Michigan, USA), Andrew Hayen (University of Technology Sydney, Australia), Paul Boutros (Ontario Institute of Cancer Research, Toronto, Ontario, Canada).

Clinical Research Partners' IT Experts: Wei Guo (Johns Hopkins University, The James Buchanan Brady Urological Institute, Baltimore, USA), Nicole Benfante (Memorial Sloan Kettering Cancer Center, New York, USA), Janet Cowan (University of California San Francisco, San Francisco, USA), Dattatraya Patil (Emory University School of Medicine, Winship Cancer Institute, Atlanta, USA), Emily Tolosa (MD Anderson Cancer Centre, Houston, Texas, USA), Tae-Kyung Kim (University of Michigan and Michigan Urological Surgery Improvement Collaborative, Ann Arbor, Michigan, USA), Alexandre Mamedov (University of Toronto, Sunnybrook Health Sciences Centre, Toronto, Ontario, Canada), Vincent LaPointe (University of British Columbia, BC Cancer Agency, Vancouver, Canada), Trafford Crump (University of Calgary, Southern Alberta Institute of Urology, Calgary, Canada), Vasilis Stavrinides (University College London & University College London Hospital Trust, London, UK), Jenna Kimberly-Duffell (University of

Cambridge & Cambridge University Hospitals NHS Foundation Trust, Cambridge, UK), Aida Santaolalla (King's College London, London, UK & Guy's and St Thomas' NHS Foundation Trust, London, UK), Daan Nieboer (Erasmus Medical Center, Rotterdam, The Netherlands), Jonathan Olivier (Lille University Hospital Center, Lille, France), Tiziana Rancati (Fondazione IRCCS Istituto Nazionale dei Tumori di Milano, Milan, Italy), Helén Ahlgren (Sahlgrenska University Hospital, Göteborg, Sweden), Juanma Mascarós (Instituto Valenciano de Oncología, Valencia, Spain), Annica Löfgren (Skåne University Hospital, Malmö, Sweden), Kurt Lehmann (Kantonsspital Baden, Baden, Switzerland), Catherine Han Lin (Monash University and Epworth HealthCare, Melbourne, Australia), Hiromi Hirama (Kagawa University, Kagawa, Japan), Kwang Suk Lee (Yonsei University College of Medicine, Gangnam Severance Hospital, Seoul, Korea).

Research Advisory Committee: Guido Jenster (Erasmus MC, Rotterdam, the Netherlands), Anssi Auvinen (University of Tampere, Tampere, Finland), Anders Bjartell (Skåne University Hospital, Malmö, Sweden), Masoom Haider (University of Toronto, Toronto, Canada), Kees van Bochove (The Hyve B.V. Utrecht, Utrecht, the Netherlands), Ballentine Carter (Johns Hopkins University, Baltimore, USA – until 2018).

Management team: Sam Gledhill (Movember Foundation, Melbourne, Australia), Mark Buzza / Michelle Kouspou (Movember Foundation, Melbourne, Australia), Chris Bangma (Erasmus Medical Center, Rotterdam, The Netherlands), Monique Roobol (Erasmus Medical Center, Rotterdam, The Netherlands), Sophie Bruinsma / Jozien Helleman (Erasmus Medical Center, Rotterdam, The Netherlands).

References

1. Epstein JI, Egevad L, Amin MB, Delahunt B, Srigley JR, Humphrey PA. The 2014 international society of urological pathology (ISUP) consensus conference on Gleason grading of prostatic carcinoma. *The American journal of surgical pathology* 2016;40(2):244–52.

2. Pearson JD, Morrell CH, Landis PK, Carter HB, Brant LJ. Mixed-effects regression models for studying the natural history of prostate disease. *Statistics in Medicine* 1994;13(5-7):587–601.

3. Lin H, McCulloch CE, Turnbull BW, Slate EH, Clark LC. A latent

class mixed model for analysing biomarker trajectories with irregularly scheduled observations. *Statistics in Medicine* 2000;19(10):1303–18.

4. De Boor C. A practical guide to splines; vol. 27. Springer-Verlag New York; 1978.

5. Eilers PH, Marx BD. Flexible smoothing with B-splines and penalties. *Statistical Science* 1996;11(2):89–121.

6. Tsiatis AA, Davidian M. Joint modeling of longitudinal and time-to-event data: an overview. *Statistica Sinica* 2004;14(3):809–34.

7. Gentleman R, Geyer CJ. Maximum likelihood for interval censored data: Consistency and computation. *Biometrika* 1994;81(3):618–23.

8. Bruinsma SM, Zhang L, Roobol MJ, Bangma CH, Steyerberg EW, Nieboer D, Van Hemelrijck M, consortium MFGAPPCASG, Trock B, Ehdaie B, et al. The Movember foundation's GAP3 cohort: a profile of the largest global prostate cancer active surveillance database to date. *BJU international* 2018;121(5):737–44.

9. Turnbull BW. The empirical distribution function with arbitrarily grouped, censored and truncated data. *Journal of the Royal Statistical Society Series B (Methodological)* 1976;38(3):290–5.

10. Rizopoulos D. The R package JMbayes for fitting joint models for longitudinal and time-to-event data using MCMC. *Journal of Statistical Software* 2016;72(7):1–46.

11. Rizopoulos D, Molenberghs G, Lesaffre EM. Dynamic predictions with time-dependent covariates in survival analysis using joint modeling and landmarking. *Biometrical Journal* 2017;59(6):1261–76.

12. Steyerberg EW, Vickers AJ, Cook NR, Gerds T, Gonen M, Obuchowski N, Pencina MJ, Kattan MW. Assessing the performance of prediction models: a framework for some traditional and novel measures. *Epidemiology (Cambridge, Mass)* 2010;21(1):128.

13. Bokhorst LP, Alberts AR, Rannikko A, Valdagni R, Pickles T, Kakehi Y, Bangma CH, Roobol MJ, PRIAS study group . Compliance rates with the Prostate Cancer Research International Active Surveillance (PRIAS)

protocol and disease reclassification in noncompliers. *European Urology* 2015;68(5):814–21.

14. Nieboer D, Tomer A, Rizopoulos D, Roobol MJ, Steyerberg EW. Active surveillance: a review of risk-based, dynamic monitoring. *Translational andrology and urology* 2018;7(1):106–15.

15. de Carvalho TM, Heijnsdijk EA, de Koning HJ. Estimating the risks and benefits of active surveillance protocols for prostate cancer: a microsimulation study. *BJU international* 2017;119(4):560–6.